ORBITAL-FREE DENSITY FUNCTIONAL THEORY USING HIGHER-ORDER FINITE DIFFERENCES

A Thesis
Presented to
The Academic Faculty

by

Swarnava Ghosh

In Partial Fulfillment
of the Requirements for the Degree
Master of Science in the
School of Civil and Environmental Engineering

Georgia Institute of Technology
May 2015

ORBITAL-FREE DENSITY FUNCTIONAL THEORY USING HIGHER-ORDER FINITE DIFFERENCES

Approved by:

Dr. Phanish Suryanarayana, Advisor
School of Civil and Environmental Engineering
Georgia Institute of Technology

Dr. Glaucio H. Paulino
School of Civil and Environmental Engineering
Georgia Institute of Technology
University of Illinois at Urbana-Champaign

Dr. Arash Yavari
School of Civil and Environmental Engineering
Georgia Institute of Technology

Date Approved: 20 April 2015

Dedicated to my parents

for their constant encouragement and support.

ACKNOWLEDGEMENTS

I would like to express my deepest gratitude to my advisor Professor Phanish Suryanarayana. His continuous support, constant encouragement and deep insights into the subject has been tremendously valuable for me. I am deeply indebt to him for the time and effort he has dedicated to mentoring my research. I am also grateful to Professor Glaucio H. Paulino and Professor Arash Yavari for serving on my committee and providing feedback on this thesis.

I would like to express my gratitude to Deepa Phanish for developing an initial framework on which this present work is based.

I have been fortunate enough to be in an excellent company of friends. I would like to thank Pradeep, Sarvani, Lakshmi, Ajinkya, Oguzhan, Souhayl, Arkadeep, Anish, Dhwanil, Sourav, Monodeep, Suvadeep, Arindam, Abhishek, Samantak, Abhinav. I would also like to thank Aruni, Sumon and Aditya for the excellent friendship that we share.

I will always be grateful to my parents, grandparents, uncles, aunts and cousins. My parents have been the most encouraging when I decided to pursue a career in scientific research. This would not have been possible without their support and encouragement. I would also like to thank Sreya for being very supportive and understanding.

TABLE OF CONTENTS

LIST OF TABLES

LIST OF FIGURES

SUMMARY

Density functional theory (DFT) is not only an accurate but also a widely used theory for describing the quantum-mechanical electronic structure of matter. In this approach, the intractable problem of interacting electrons is simplified to a tractable problem of non-interacting electrons moving in an effective potential. Even with this simplification, DFT remains extremely computationally expensive. In particular, DFT scales cubically with respect to the number of atoms, which restricts the size of systems that can be studied. Orbital free density functional theory (OF-DFT) represents a simplification of DFT applicable to metallic systems that behave like a free-electron gas.

Current implementations of OF-DFT employ the plane-wave basis, the global nature of the basis prevents the efficient use of modern high-performance computer architectures. We present a real-space formulation and higher-order finite-difference implementation of periodic Orbital-free Density Functional Theory (OF-DFT). Specifically, utilizing a local reformulation of the electrostatic and kernel terms, we develop a generalized framework suitable for performing OF-DFT simulations with different variants of the electronic kinetic energy. In particular, we develop a self-consistent field (SCF) type fixed-point method for calculations involving linear-response kinetic energy functionals. In doing so, we make the calculation of the electronic ground-state and forces on the nuclei amenable to computations that altogether scale linearly with the number of atoms. We develop a parallel implementation of our method using Portable, Extensible Toolkit for scientific computations (PETSc) suite of data structures and routines. The communication between processors is handled via the Message Passing

Interface (MPI). We implement this formulation using the finite-difference discretization, using which we demonstrate that higher-order finite-differences can achieve relatively large convergence rates with respect to mesh-size in both the energies and forces. Additionally, we establish that the fixed-point iteration converges rapidly, and that it can be further accelerated using extrapolation techniques like Anderson mixing. We verify the accuracy of our results by comparing the energies and forces with plane-wave methods for selected examples, one of which is the vacancy formation energy in Aluminum. Overall, we demonstrate that the proposed formulation and implementation is an attractive choice for performing OF-DFT calculations.

CHAPTER I

INTRODUCTION

Electronic structure calculations play a vital role in modeling phenomena involving formation and/or breaking of chemical bonds. The fundamental equation describing the electronic structure of matter is the Schrödinger equation. However, solution of the Schrödinger equation is immensely expensive and this hinders the size of system that can be studied to tens of electrons [38]. Several approaches have been proposed that reduces the computational cost of the Schrodinger equation, including the seminal work of Hohenberg and Kohn [30]. In their work, Hohenberg and Kohn [30] proved the existence of a one-to-one correspondence between the ground state electron density and the ground state wavefunction of a many body system, thereby replacing the ground state wavefunction with the ground state electron density as the fundamental unknown field. This greatly reduces the dimensionality and complexity of the problem.

Kohn-Sham Density Functional Theory (DFT) [30, 39] has a relatively high accuracy/cost ratio, which makes it a popular electronic structure theory for predicting material properties and behavior. In DFT, the system of interacting electrons is replaced with a system of non-interacting electrons moving in an effective potential [45, 13]. The electronic ground-state in DFT is typically determined by solving for the Kohn-Sham orbitals, the number of which is commensurate with the size of the system, i.e. number of electrons [13, 42]. Since these orbitals need to be orthonormal, the overall solution procedure scales cubically with the number of atoms [13, 42]. In order to overcome this restrictive scaling, significant research has focused on the development of linear-scaling methods [24, 7]. Nearly all of these approaches, in one

form or the other, employ the decay of the density matrix [5] in conjunction with truncation to achieve linear-scaling [24, 7]. However, an efficient linear-scaling algorithm for metallic systems still remains an open problem [9].

Orbital-free DFT (OF-DFT) represents a simplified version of DFT, wherein the electronic kinetic energy is modeled using a functional of the electron density [61]. Commonly used kinetic energy functionals include the Thomas-Fermi-von Weizsacker (TFW) [59, 16, 64], Wang-Teter (WT) [60] and Wang, Govind & Carter (WGC) [62, 63] functionals. Amongst these, the WT and WGC energies are designed so as to match the linear-response of a homogeneous electron gas [61]. Previous studies have shown that OF-DFT is able to provide an accurate description of systems whose electronic structure resembles a free-electron gas e.g. Aluminum and Magnesium [10, 28, 31]. There have been recent efforts to extend the applicability of OF-DFT to covalently bonded materials [66] as well as molecular systems [65]. In essence, OF-DFT can be viewed as a 'single-orbital' version of DFT, wherein the cubic-scaling bottleneck arising from orthogonalization is no longer applicable. In addition to this, OF-DFT possesses an extremely favorable scaling with respect to temperature compared to DFT [53, 37]. Overall, OF-DFT has the potential to enable electronic structure calculations for system sizes that are intractable for DFT.

The plane-wave basis is attractive for performing OF-DFT calculations [60, 29, 34] because of the spectral convergence with increasing basis size and the efficient evaluation of convolutions using the Fast Fourier Transform (FFT) [14]. However, the development of implementations which can efficiently utilize modern large-scale, distributed-memory computer architectures is particularly challenging. Further, evaluation of the electrostatic terms within the plane-wave basis typically scales quadratically with the number of atoms [32]. In view of this, recent efforts have been directed towards developing real-space approaches for OF-DFT, including finite-differences [57] and finite-elements [21, 44]. Amongst these, the finite-element method provides

the flexibility of an adaptive discretization. This attribute has been employed to perform all-electron calculations [21, 44] and to develop a coarse-grained formulation of OF-DFT for studying crystal defects [20]. However, higher-order finite-differences — which have been shown to be extremely efficient in non-periodic OF-DFT with the TFW kinetic energy functional [57] — remain unexplored in the context of periodic OF-DFT simulations, particularly when linear-response kinetic energy functionals like WT and WGC are employed.

The electronic ground state in OF-DFT can be expressed as the solution of a non-linear, constrained minimization problem [18, 4, 6, 8, 21, 57]. The approaches which have previously been employed to solve this problem include variants of conjugate-gradient [29, 21, 35, 57] and Newton [29, 18, 44] methods. In these approaches, the techniques used to enforce the constraints include Lagrange multipliers [33, 44], the penalty method [21] and the Augmented-Lagrangian method [57]. We present a local real-space formulation and implementation of periodic OF-DFT[22]. In particular, a fixed-point iteration with respect to the kernel potential for simulations involving linear-response kinetic energy functionals and a parallel implementation of the proposed method in the framework of higher-order finite-differences is developed. We demonstrate the robustness, efficiency and accuracy of the proposed approach through selected examples, the results of which are compared against existing plane-wave methods. The remainder of this thesis is organized as follows. We introduce OF-DFT in Chapter 2 and discuss its real-space formulation in Chapter 3. Subsequently, we describe the numerical implementation in Chapter 4, which we verify through examples in Chapter 5. Finally, we conclude in Chapter 6.

CHAPTER II

ORBITAL-FREE DENSITY FUNCTIONAL THEORY

In this chapter, we present a generalized mathematical framework of the Orbital-Free Density Functional Theory. We start by considering a charge neutral system of M_a atoms and N_e electrons in a cuboidal domain Ω under periodic boundary conditions. Let $\mathbf{R} = \{\mathbf{R}_1, \mathbf{R}_2, \ldots, \mathbf{R}_{M_a}\}$ denote the positions of the nuclei with charges $\mathbf{Z} = \{Z_1, Z_2, \ldots, Z_{M_a}\}$ respectively. The energy of this system as described by OF-DFT is [45]

$$\mathcal{E}(u, \mathbf{R}) = T_s(u) + E_{xc}(u) + E_H(u) + E_{ext}(u, \mathbf{R}) + E_{zz}(\mathbf{R})\,, \tag{1}$$

where $u = \sqrt{\rho}$, ρ being the electron density. $E_{xc}(u)$ is the exchange-correlation energy. $E_H(u)$, $E_{ext}(u, \mathbf{R})$, $E_{zz}(\mathbf{R})$ is the electrostatic interaction energies between electron-electron, electron-nuclei and the nuclei-nuclei respectively. Introducing the parameters λ and $\mu \in \{0, 1\}$ so that different variants of the electronic kinetic energy $T_s(u)$ can be encompassed within a single expression, we can write

$$T_s(u) = T_{TF}(u) + \lambda T_{vW}(u) + \mu T_{LR}(u)\,, \tag{2}$$

where $T_{TF}(u)$ is the Thomas-Fermi energy [59, 16], $T_{vW}(u)$ is the von Weizsacker [64] term and $T_{LR}(u)$ is a non-local kernel energy incorporated to make the kinetic energy satisfy the linear-response of a homogeneous electron gas [61]. They can be represented as

$$T_{TF}(u) = C_F \int_\Omega u^{10/3}(\mathbf{x})\,\mathrm{d}\mathbf{x}\,, \tag{3}$$

$$T_{vW}(u) = \frac{1}{2}\int_\Omega |\nabla u(\mathbf{x})|^2\,\mathrm{d}\mathbf{x}\,, \tag{4}$$

$$T_{LR}(u) = C_F \int_{\mathbb{R}^3}\int_\Omega u^{2\alpha}(\mathbf{x})\, K(|\mathbf{x}-\mathbf{x}'|, \rho(\mathbf{x}), \rho(\mathbf{x}'))\, u^{2\beta}(\mathbf{x}')\mathrm{d}\mathbf{x}\mathrm{d}\mathbf{x}'\,, \tag{5}$$

where α and β are parameters, and the constant $C_F = \frac{3}{10}(3\pi^2)^{\frac{2}{3}}$. On the one hand, the Thomas-Fermi-von Weizsacker (TFW) family of functionals with the adjustable parameter λ is obtained by setting $\mu = 0$ [45]. On the other hand, kinetic energy functionals which satisfy the Lindhard susceptibility function are obtained by setting $\mu = \lambda = 1$ with appropriate choices of α, β and the kernel $K(|\mathbf{x}-\mathbf{x}'|, \rho(\mathbf{x}), \rho(\mathbf{x}'))$ [61]. In particular, the Wang & Teter (WT) functional [60] utilizes a density independent kernel, whereas the Wang, Govind & Carter (WGC) functional [62, 63] employs a density dependent kernel. It is common to perform a Taylor series expansion of the density dependent kernel $K(|\mathbf{x}-\mathbf{x}'|, \rho(\mathbf{x}), \rho(\mathbf{x}'))$ about the average electron density $\bar{\rho}$ [63]. On doing so, we arrive at

$$\begin{aligned} T_{LR}(u) &= C_F \sum_{m=0}^{L} \sum_{n=0}^{L} \sum_{p=0}^{m} \sum_{q=0}^{n} C_{mnpq} \\ &\int_{\mathbb{R}^3} \int_{\Omega} u^{2(m-p+\alpha)}(\mathbf{x}) K_{mn}(|\mathbf{x}-\mathbf{x}'|) u^{2(n-q+\beta)}(\mathbf{x}') \, \mathrm{d}\mathbf{x} \, \mathrm{d}\mathbf{x}' \,, \end{aligned} \tag{6}$$

where L is the order of the expansion, the coefficients

$$C_{mnpq} = \frac{(-1)^{p+q}}{m!\, n!} \binom{m}{p} \binom{n}{q} \bar{\rho}^{p+q-m-n} \,, \tag{7}$$

and the kernels

$$K_{mn}(|\mathbf{x}-\mathbf{x}'|) = \bar{\rho}^{m+n} \left(\frac{\partial^{m+n} K(|\mathbf{x}-\mathbf{x}'|, \rho(\mathbf{x}), \rho(\mathbf{x}'))}{\partial \rho^m(\mathbf{x}) \partial \rho^n(\mathbf{x}')} \right) \Bigg|_{\rho=\bar{\rho}} . \tag{8}$$

The second term in Eqn. 1 is referred to as the exchange-correlation energy. It is generally modeled in OF-DFT using the local density approximation (LDA) [39]:

$$E_{xc}(u) = \int_{\Omega} \varepsilon_{xc}(u(\mathbf{x})) u^2(\mathbf{x}) \, \mathrm{d}\mathbf{x} \,, \tag{9}$$

where $\varepsilon_{xc}(u) = \varepsilon_x(u) + \varepsilon_c(u)$ is the sum of the exchange and correlation per particle of a uniform electron gas of density $\rho = u^2$. Employing the Perdew-Zunger [48] parameterization of the correlation energy calculated by Ceperley-Alder [11], the

exchange and correlation functionals can be represented as

$$\varepsilon_x(u) = -\frac{3}{4}\left(\frac{3}{\pi}\right)^{1/3} u^{2/3}\,, \tag{10}$$

$$\varepsilon_c(u) = \begin{cases} \frac{\gamma_1}{1+\beta_1\sqrt{r_s}+\beta_2 r_s} & r_s \geq 1 \\ A_1 \log r_s + B_1 + C_1 r_s \log r_s + D_1 r_s & r_s < 1 \end{cases} \tag{11}$$

where $r_s = (\frac{3}{4\pi u^2})^{1/3}$, and the constants $\gamma_1 = -0.1423$, $\beta_1 = 1.0529$, $\beta_2 = 0.3334$, $A_1 = 0.0311$, $B_1 = -0.048$, $C_1 = 0.002$ and $D_1 = -0.0116$.

The final three terms in Eqn. 1 represent electrostatic energies [42]. In periodic systems, they can be expressed as

$$E_H(u) = \frac{1}{2}\int_{\mathbb{R}^3}\int_{\Omega} \frac{u^2(\mathbf{x})u^2(\mathbf{x}')}{|\mathbf{x}-\mathbf{x}'|}\,\mathrm{d}\mathbf{x}\,\mathrm{d}\mathbf{x}'\,, \tag{12}$$

$$E_{ext}(u,\mathbf{R}) = \sum_I \int_{\Omega} u^2(\mathbf{x}) V_I(\mathbf{x},\mathbf{R}_I)\,\mathrm{d}\mathbf{x}\,, \tag{13}$$

$$E_{zz}(\mathbf{R}) = \frac{1}{2}\sum_I \sum_{\substack{J_\Omega \\ J_\Omega \neq I}} \frac{Z_I Z_{J_\Omega}}{|\mathbf{R}_I - \mathbf{R}_{J_\Omega}|}\,, \tag{14}$$

where the summation over I and J_Ω signifies all atoms in $\mathbb{R}^3$ and Ω respectively. The Hartree energy $E_H(u)$ is the classical interaction energy of the electron density, $V_I(\mathbf{x},\mathbf{R}_I)$ is the potential due to the nucleus positioned at $\mathbf{R}_I$, $E_{ext}(u,\mathbf{R})$ is the interaction energy between the electron density and the nuclei, and $E_{zz}(\mathbf{R})$ is the repulsion energy between the nuclei.

The ground state of the system in OF-DFT is given by the variational problem [4, 21, 18, 8, 57]

$$\mathcal{E}_0 = \inf_{\mathbf{R}\in\mathbb{R}^{3M_a}} \inf_{u\in\mathcal{X}} \mathcal{E}(u,\mathbf{R})\,, \quad \mathcal{X} = \{u : u \in X,\, u \geq 0,\, \mathcal{C}(u) = 0\}\,, \tag{15}$$

where X is some appropriate space of periodic functions and

$$\mathcal{C}(u) = \int_{\Omega} u^2(\mathbf{x})\,\mathrm{d}\mathbf{x} - N_e \tag{16}$$

represents the constraint on the total number of electrons. The inequality constraint $u \geq 0$ is to ensure that u is nodeless, i.e. does not possess a zero crossing. In this

work, we focus on developing a local formulation and higher-order finite-difference implementation for determining the ground-state in periodic OF-DFT simulations.

CHAPTER III

REAL-SPACE FORMULATION

In this chapter, we develop a periodic OF-DFT formulation that is amenable to a linear-scaling real-space implementation. First, we present a local description of the kernel energy and potential in Section 3.1. Next, we discuss rewriting of the electrostatic terms into a local form in Section 3.2. Finally, we incoporate these local representations into a framework for determining the OF-DFT ground-state in Section 3.3.

3.1 Local reformulation of the kernel energy and potential

In simulations where linear-response kinetic energy functionals are employed, the kernel energy $T_{LR}(u)$ as well as the kernel potential

$$\begin{aligned} V_{LR}(\mathbf{x}) &= \frac{\delta T_{LR}(u)}{\delta u^2} \\ &= C_F \sum_{m=0}^{L}\sum_{n=0}^{L}\sum_{p=0}^{m}\sum_{q=0}^{n} C_{mnpq} \\ &\quad \Bigg[(m-p+\alpha)u^{2(m-p+\alpha-1)}(\mathbf{x})\int_{\mathbb{R}^3} K_{mn}(|\mathbf{x}-\mathbf{x}'|)u^{2(n-q+\beta)}(\mathbf{x}')\,\mathrm{d}\mathbf{x}' \\ &+ \quad (n-q+\beta)u^{2(n-q+\beta-1)}(\mathbf{x})\int_{\mathbb{R}^3} K_{mn}(|\mathbf{x}-\mathbf{x}'|)u^{2(m-p+\alpha)}(\mathbf{x}')\,\mathrm{d}\mathbf{x}'\Bigg], \quad (17) \end{aligned}$$

are inherently non-local in real-space. In order to enable a linear-scaling implementation, we start by defining the potentials

$$V_{mnq\beta}(\mathbf{x}) = \int_{\mathbb{R}^3} K_{mn}(|\mathbf{x}-\mathbf{x}'|)u^{2(n-q+\beta)}(\mathbf{x}')\,\mathrm{d}\mathbf{x}'\,, \quad (18)$$

$$V_{mnp\alpha}(\mathbf{x}) = \int_{\mathbb{R}^3} K_{mn}(|\mathbf{x}-\mathbf{x}'|)u^{2(m-p+\alpha)}(\mathbf{x}')\,\mathrm{d}\mathbf{x}'\,. \quad (19)$$

After approximating the kernels $K_{mn}(|\mathbf{x}-\mathbf{x}'|)$ in Fourier space using rational functions [12], we arrive at

$$V_{mnq\beta}(\mathbf{x}) = \sum_{r=1}^{R} V_{mnq\beta r}(\mathbf{x})\,, \tag{20}$$

$$V_{mnp\alpha}(\mathbf{x}) = \sum_{r=1}^{R} V_{mnp\alpha r}(\mathbf{x})\,, \tag{21}$$

where $V_{mnq\beta r}(\mathbf{x})$ and $V_{mnp\alpha r}(\mathbf{x})$ are solutions of the Helmholtz equations

$$-\frac{1}{(2\bar{k}_F)^2}\nabla^2 V_{mnq\beta r}(\mathbf{x}) + Q_{mnr} V_{mnq\beta r}(\mathbf{x}) = P_{mnr} f_{mp\alpha}(\mathbf{x})\,, \tag{22}$$

$$-\frac{1}{(2\bar{k}_F)^2}\nabla^2 V_{mnp\alpha r}(\mathbf{x}) + Q_{mnr} V_{mnp\alpha r}(\mathbf{x}) = P_{mnr} f_{nq\beta}(\mathbf{x})\,, \tag{23}$$

under periodic boundary conditions and appropriate choice of complex constants P_{mnr} and Q_{mnr}. Above, $\bar{k}_F = (3\pi^2\bar{\rho})^{\frac{1}{3}}$ and

$$f_{mp\alpha}(\mathbf{x}) = \begin{cases} -\frac{1}{(2\bar{k}_F)^2}\nabla^2 u^{2(m-p+\alpha)}(\mathbf{x}) & \text{if } m = n = 0\,, \\ u^{2(m-p+\alpha)}(\mathbf{x}) & \text{otherwise}\,, \end{cases} \tag{24}$$

$$f_{nq\beta}(\mathbf{x}) = \begin{cases} -\frac{1}{(2\bar{k}_F)^2}\nabla^2 u^{2(n-q+\beta)}(\mathbf{x}) & \text{if } m = n = 0\,, \\ u^{2(n-q+\beta)}(\mathbf{x}) & \text{otherwise}\,. \end{cases} \tag{25}$$

Thereafter, the kernel potential $V_{LR}(\mathbf{x})$ and the corresponding kernel energy $T_{LR}(u)$ can be calculated in linear-scaling fashion using the expressions

$$\begin{aligned} V_{LR}(\mathbf{x}) = {} & C_F \sum_{m=0}^{L}\sum_{n=0}^{L}\sum_{p=0}^{m}\sum_{q=0}^{n}\sum_{r=1}^{R} C_{mnpq}\Big[(m-p+\alpha)u^{2(m-p+\alpha-1)}(\mathbf{x})V_{mnq\beta r}(\mathbf{x}) \\ & + (n-q+\beta)u^{2(n-q+\beta-1)}(\mathbf{x})V_{mnp\alpha r}(\mathbf{x})\Big]\,, \end{aligned} \tag{26}$$

$$\begin{aligned} T_{LR}(u) = {} & \frac{1}{2}C_F \sum_{m=0}^{L}\sum_{n=0}^{L}\sum_{p=0}^{m}\sum_{q=0}^{n}\sum_{r=1}^{R} C_{mnpq}\int_{\Omega}\Big[u^{2(m-p+\alpha)}(\mathbf{x})V_{mnq\beta r}(\mathbf{x}) \\ & + u^{2(n-q+\beta)}(\mathbf{x})V_{mnp\alpha r}(\mathbf{x})\Big]\,\mathrm{d}\mathbf{x} \end{aligned} \tag{27}$$

where $V_{mnq\beta r}(\mathbf{x})$ and $V_{mnp\alpha r}(\mathbf{x})$ are solutions of the Helmholtz equations given in Eqns. 22 and 23 respectively.

3.2 Local reformulation of the electrostatics

The electrostatic terms given in Eqns. 12, 13 and 14 are non-local in real-space. Further, they are individually divergent in periodic systems. To overcome this, we introduce the charge density of the nuclei [46, 56, 21, 54, 55, 57]:

$$b(\mathbf{x},\mathbf{R}) = \sum_J b_J(\mathbf{x},\mathbf{R}_J)\ , \quad b_J(\mathbf{x},\mathbf{R}_J) = \frac{-1}{4\pi}\nabla^2 V_J(\mathbf{x},\mathbf{R}_J)\,, \tag{28}$$

where $b_J(\mathbf{x},\mathbf{R}_J)$ is the charge density of the J^{th} nucleus, and the summation over J extends to all atoms in $\mathbb{R}^3$. In OF-DFT calculations, it is common to remove the core electrons and replace the singular Coulomb potential with an effective potential $V_J(\mathbf{x},\mathbf{R}_J)$, referred to as the pseudopotential approximation [49]. The absence of orbitals in OF-DFT requires that the pseudopotential be local, i.e. $V_J(\mathbf{x},\mathbf{R}_J)$ depends only on the distance from the nucleus. Since the pseudopotential replicates the Coulomb potential outside the core cutoff radius r_c, $b_J(\mathbf{x},\mathbf{R}_J)$ has a compact support within a ball of radius r_c centered at $\mathbf{R}_J$ [46, 57]. In this framework, it follows that

$$\int_{\mathbb{R}^3} b_J(\mathbf{x},\mathbf{R}_J)\,\mathrm{d}\mathbf{x} = Z_J\,, \quad \int_\Omega b(\mathbf{x},\mathbf{R})\,\mathrm{d}\mathbf{x} = N_e\,. \tag{29}$$

Using the above definition for the charge density of the nuclei, we can rewrite the total electrostatic energy as the following variational problem

$$\begin{aligned} & E_H(u) + E_{ext}(u,\mathbf{R}) + E_{zz}(\mathbf{R}) \\ = \ & \sup_{\phi\in Y}\left\{ -\frac{1}{8\pi}\int_\Omega |\nabla\phi(\mathbf{x})|^2\,\mathrm{d}\mathbf{x} + \int_\Omega (u^2(\mathbf{x}) + b(\mathbf{x},\mathbf{R}))\phi(\mathbf{x})\,\mathrm{d}\mathbf{x}\right\} \\ - \ & \frac{1}{2}\sum_J \int_\Omega b_J(\mathbf{x},\mathbf{R}_J)V_J(\mathbf{x},\mathbf{R}_J)\,\mathrm{d}\mathbf{x} + \mathcal{E}_c^*(\mathbf{R})\,, \end{aligned} \tag{30}$$

where $\phi(\mathbf{x})$ is the electrostatic potential, Y is some appropriate space of periodic functions, the second last term accounts for the self energy of the nuclei and the last term corrects for overlapping charge density of nuclei. We comment here that the second term is indeed local because of the fact that b_J is compactly supported. A detailed discussion on the nature of $\mathcal{E}_c^*(\mathbf{R})$ and its evaluation can be found in

Appendix B. With this reformulation of the total electrostatic energy, we arrive at the variational problem

$$\mathcal{E}(u,\mathbf{R}) = \left\{ \sup_{\phi\in Y} \mathcal{F}(u,\mathbf{R},\phi) + \mu T_{LR}(u) \right\}, \tag{31}$$

where the functional

$$\begin{aligned} \mathcal{F}(u,\mathbf{R},\phi) \;=\; & C_F \int_\Omega u^{10/3}(\mathbf{x})\,\mathrm{d}\mathbf{x} + \frac{\lambda}{2}\int_\Omega |\nabla u(\mathbf{x})|^2\,\mathrm{d}\mathbf{x} + \int_\Omega \varepsilon_{xc}(u(\mathbf{x}))u^2(\mathbf{x})\,\mathrm{d}\mathbf{x} \\ & -\frac{1}{8\pi}\int_\Omega |\nabla\phi(\mathbf{x})|^2\,\mathrm{d}\mathbf{x} + \int_\Omega (u^2(\mathbf{x}) + b(\mathbf{x},\mathbf{R}))\phi(\mathbf{x})\,\mathrm{d}\mathbf{x} \\ & -\frac{1}{2}\sum_J \int_\Omega b_J(\mathbf{x},\mathbf{R}_J)V_J(\mathbf{x},\mathbf{R}_J)\,\mathrm{d}\mathbf{x} + \mathcal{E}_c^*(\mathbf{R})\,. \end{aligned} \tag{32}$$

3.3 OF-DFT ground-state

In the above described framework, the variational problem for determining the ground-state in OF-DFT can be written as

$$\mathcal{E}_0 = \inf_{\mathbf{R}\in\mathbb{R}^{3M_a}} \mathcal{E}^*(\mathbf{R})\,, \tag{33}$$

where

$$\mathcal{E}^*(\mathbf{R}) = \inf_{u\in\mathcal{X}} \mathcal{E}(u,\mathbf{R}) = \inf_{u\in\mathcal{X}} \left\{ \sup_{\phi\in Y} \mathcal{F}(u,\mathbf{R},\phi) + \mu T_{LR}(u) \right\}. \tag{34}$$

Through this decomposition, the ground-state can be ascertained by solving the electronic structure problem in Eqn. 34 for every configuration of the nuclei encountered during the geometry optimization described by Eqn. 33. Below, we discuss local real-space approaches for each of these variational problems.

3.3.1 Electronic structure problem

Consider the variational problem in Eqn. 34 for determining the electronic ground-state. On taking the first variation, we arrive at the Euler-Lagrange equation

$$\mathcal{H}u(\mathbf{x}) = \eta u(\mathbf{x})\,, \quad \mathcal{H} = -\frac{\lambda}{2}\nabla^2 + \left(V_{TF}(\mathbf{x}) + \mu V_{LR}(\mathbf{x}) + V_{xc}(\mathbf{x}) + \phi(\mathbf{x}) \right), \tag{35}$$

where η is a Lagrange multiplier used to enforce the constraint $\mathcal{C}(u) = 0$. Further, $V_{LR}(\mathbf{x})$ is given by Eqn. 26, $\phi(\mathbf{x})$ is the solution of the Poisson equation

$$\frac{-1}{4\pi}\nabla^2\phi(\mathbf{x}) = u^2(\mathbf{x}) + b(\mathbf{x},\mathbf{R}) \tag{36}$$

under periodic boundary conditions and

$$V_{TF}(\mathbf{x}) = \frac{\delta T_{TF}(u)}{\delta u^2} = \frac{5}{3}C_F u^{4/3}(\mathbf{x})\,, \tag{37}$$

$$V_{xc}(\mathbf{x}) = \frac{\delta E_{xc}(u)}{\delta u^2} = V_x(\mathbf{x}) + V_c(\mathbf{x})\,. \tag{38}$$

In the above equation, $V_{xc}(\mathbf{x})$ is the exchange-correlation potential with

$$V_x(\mathbf{x}) = -\left(\frac{3}{\pi}\right)^{1/3} u^{2/3}(\mathbf{x})\,, \tag{39}$$

$$V_c(\mathbf{x}) = \begin{cases} \frac{\gamma_1+\frac{7}{6}\gamma_1\beta_1\sqrt{r_s(\mathbf{x})}+\frac{4}{3}\gamma_1\beta_2 r_s(\mathbf{x})}{(1+\beta_1\sqrt{r_s(\mathbf{x})}+\beta_2 r_s(\mathbf{x}))^2}\,, & r_s(\mathbf{x}) \geq 1 \\ \left(A_1 + \frac{2}{3}C_1 r_s(\mathbf{x})\right)\log r_s(\mathbf{x}) + \left(B_1 - \frac{1}{3}A_1\right) + \frac{1}{3}(2D_1 - C_1)r_s(\mathbf{x})\,, r_s(\mathbf{x}) < 1 \end{cases} \tag{40}$$

being the exchange and correlation potentials respectively. Even though the notation does not make it explicit, the dependence of $\mathcal{H}$ on u makes Eqn. 35 a non-linear problem. Also, since

$$\int_\Omega (\rho(\mathbf{x}) + b(\mathbf{x},\mathbf{R}))\,\mathrm{d}\mathbf{x} = 0\,, \tag{41}$$

the Poisson equation in Eqn. 36 with periodic boundary conditions is a well-posed problem.

The electronic ground-state can be determined by solving the non-linear eigenvalue problem in Eqn. 35 for the eigenfunction corresponding to the lowest eigenvalue. Irrespective of the technique and choice of kinetic energy functional, $\phi(\mathbf{x})$ needs to be recalculated for every update in $u(\mathbf{x})$. Additionally, when linear-response kinetic energy functionals are employed, $V_{LR}(\mathbf{x})$ needs to be reevaluated every time $u(\mathbf{x})$ is updated. Therefore, the solution of Eqn. 35 requires the repeated solution of the Poisson equation in Eqn. 36 and the complex-valued non-Hermitian Helmholtz equations in Eqns. 22 and 23. In view of this, the self-consistent field method (SCF)

[15] commonly employed in DFT calculations is an attractive choice because of the relatively few iterations that are typically required for convergence. However, we have found such an approach to be unstable for both the TFW and WGC kinetic energy functionals, especially as the system size is increased. Since the number of Helmholtz equations that need to be solved to determine $V_{LR}(\mathbf{x})$ can be significantly large in practice (e.g. fifty-two in this work), they are expected to completely dominate the execution time. In order to mitigate this, we present below a fixed-point method with respect to $V_{LR}(\mathbf{x})$ to determine the electronic ground-state [19]. This is similar in spirit to the SCF method , and is found to converge rapidly, as demonstrated by the examples in Chapter 5.

In simulations which employ linear-response kinetic energy functionals, we define a fixed-point problem of the form

$$V_{LR} = \mathcal{V}\big[\mathcal{U}(V_{LR})\big]\,, \tag{42}$$

where the mappings

$$\mathcal{U}(V_{LR}) = \arg\inf_{u\in\mathcal{X}}\left\{\sup_{\phi\in Y}\mathcal{F}(u,\mathbf{R},\phi) + \mu\int_{\Omega} V_{LR}(\mathbf{x})u^2(\mathbf{x})\,\mathrm{d}\mathbf{x}\right\}, \tag{43}$$

and

$$\begin{aligned}\mathcal{V}\big[u\big] &= C_F\sum_{m=0}^{L}\sum_{n=0}^{L}\sum_{p=0}^{m}\sum_{q=0}^{n}\sum_{r=1}^{R} C_{mnpq}\Big[(m-p+\alpha)u^{2(m-p+\alpha-1)}(\mathbf{x})V_{mnq\beta r}(\mathbf{x}) \\ &+ (n-q+\beta)u^{2(n-q+\beta-1)}(\mathbf{x})V_{mnp\alpha r}(\mathbf{x})\Big]\,.\end{aligned} \tag{44}$$

In the above expression, $V_{mnq\beta r}(\mathbf{x})$ and $V_{mnp\alpha r}(\mathbf{x})$ are solutions to the Helmholtz equations given in Eqns. 22 and 23 respectively. We note that the Euler-Lagrange equations of the variational problem in Eqn. 43 and the OF-DFT electronic structure problem in Eqn. 34 are identical. It follows that the solution of the fixed-point problem will correspond to the ground-state kernel potential $V^*_{LR}(\mathbf{x})$ and ground-state square-root electron density $u^*(\mathbf{x})$. In order to solve this fixed-point problem,

we treat it as a non-linear equation and adopt an iteration of the form [15, 41]

$$V_{LR,k+1} = V_{LR,k} - C_k \left(\mathcal{V}\big[\mathcal{U}(V_{LR,k})\big] - V_{LR,k} \right) , \tag{45}$$

where the index k represents the iteration number and C_k is appropriately chosen to ensure/accelerate convergence. Once the fixed-point $V^*_{LR}(\mathbf{x})$ has been determined, $u^*(\mathbf{x})$ can be calculated by solving Eqn. 43 for $V_{LR}(\mathbf{x}) = V^*_{LR}(\mathbf{x})$. In Fig. 1, we present a flowchart that outlines the aforedescribed fixed-point approach. It is worth noting that for the choice of TFW kinetic energy functional ($\mu = 0$), the solution of Eqn. 43 immediately provides the electronic ground-state.

After determining the electronic ground-state square-root electron density $u^*(\mathbf{x})$, the corresponding energy can be evaluated using the expression

$$\begin{aligned}
\mathcal{E}^*(\mathbf{R}) &= C_F \int_\Omega u^{*10/3}(\mathbf{x})\,\mathrm{d}\mathbf{x} + \frac{\lambda}{2}\int_\Omega |\nabla u^*(\mathbf{x})|^2\,\mathrm{d}\mathbf{x} + \frac{\mu}{2} C_F \sum_{m=0}^{L}\sum_{n=0}^{L}\sum_{p=0}^{m}\sum_{q=0}^{n}\sum_{r=1}^{R} C_{mnpq} \\
&\quad \int_\Omega \left[u^{*2(m-p+\alpha)}(\mathbf{x}) V^*_{mnq\beta r}(\mathbf{x}) + u^{*2(n-q+\beta)}(\mathbf{x}) V^*_{mnp\alpha r}(\mathbf{x}) \right] \mathrm{d}\mathbf{x} \\
&+ \int_\Omega \varepsilon_{xc}(u^*(\mathbf{x}))u^{*2}(\mathbf{x})\,\mathrm{d}\mathbf{x} + \frac{1}{2}\int_\Omega (u^{*2}(\mathbf{x}) + b(\mathbf{x},\mathbf{R}))\phi^*(\mathbf{x})\,\mathrm{d}\mathbf{x} \\
&- \frac{1}{2}\sum_J \int_\Omega b_J(\mathbf{x},\mathbf{R}_J) V_J(\mathbf{x},\mathbf{R}_J)\,\mathrm{d}\mathbf{x} + \mathcal{E}^*_c(\mathbf{R}) ,
\end{aligned} \tag{46}$$

where $V^*_{mnq\beta r}(\mathbf{x})$, $V^*_{mnp\alpha r}(\mathbf{x})$ and $\phi^*(\mathbf{x})$ are solutions of Eqns. 22, 23 and 36 respectively for $u(\mathbf{x}) = u^*(\mathbf{x})$.

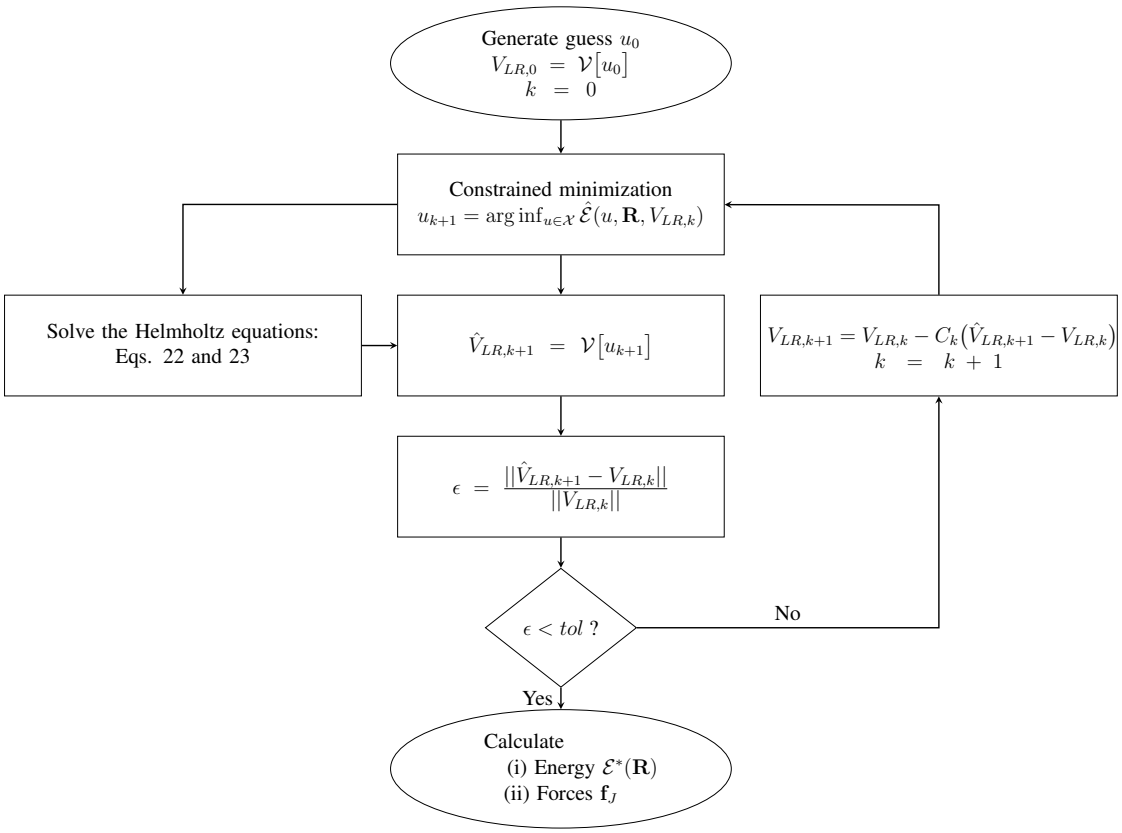

Figure 1: Fixed-point iteration for determining the electronic ground state when using linear-response kinetic energy functionals. The functional $\hat{\mathcal{E}}(u, \mathbf{R}, V_{LR,k}) = \{\sup_{\phi\in Y} \mathcal{F}(u, \mathbf{R}, \phi) + \int_\Omega V_{LR,k}(\mathbf{x})u^2(\mathbf{x})\,\mathrm{d}\mathbf{x}\}$.

3.3.2 Geometry optimization: forces on nuclei

Consider the minimization problem in Eqn. 33 for determining the equilibrium configuration of the atoms. During this geometry optimization, the forces on the nuclei can be determined using the relation

$$\begin{aligned}
\mathbf{f}_J &= -\frac{\partial \mathcal{E}^*(\mathbf{R})}{\partial \mathbf{R}_J} \\
&= -\sum_{J'} \int_\Omega \frac{\partial b_{J'}(\mathbf{x}, \mathbf{R}_{J'})}{\partial \mathbf{R}_{J'}} \left(\phi^*(\mathbf{x}) - V_{J'}(\mathbf{x}, \mathbf{R}_{J'})\right) \mathrm{d}\mathbf{x} + \mathbf{f}_\mathrm{J}^\mathrm{c}\,, \\
&= \sum_{J'} \int_\Omega \nabla b_{J'}(\mathbf{x}, \mathbf{R}_{J'}) \left(\phi^*(\mathbf{x}) - V_{J'}(\mathbf{x}, \mathbf{R}_{J'})\right) \mathrm{d}\mathbf{x} + \mathbf{f}_\mathrm{J}^\mathrm{c}\,, \qquad (47)
\end{aligned}$$

where $\mathbf{f}_J$ denotes the force on the J^{th} nucleus and the summation over J' signifies the J^{th} atom and its periodic images. Additionally, $\phi^*(\mathbf{x})$ is the solution of the Poisson

equation in Eqn. 36 for $u(\mathbf{x}) = u^*(\mathbf{x})$ and

$$\mathbf{f}_J^c = -\frac{\partial \mathcal{E}_c^*(\mathbf{R})}{\partial \mathbf{R}_J} \tag{48}$$

corrects for the error in forces due to overlapping charge density of nuclei. The expression for this correction has been derived in Appendix B. The last equality in Eqn. 47 is obtained by using the spherical symmetry of $b_{J'}(\mathbf{x}, \mathbf{R}_{J'})$. Since $\nabla b_{J'}(\mathbf{x}, \mathbf{R}_{J'})$ has compact support in a ball of radius r_c centered at $\mathbf{R}_{J'}$, only a finite number of periodic images of the J^{th} atom have an overlap with Ω. Therefore, similar to the calculation of the electronic ground state, evaluation of the forces on the nuclei is amenable to a linear-scaling real-space implementation.

CHAPTER IV

NUMERICAL IMPLEMENTATION

In this chapter, we describe a higher-order finite-difference implementation of the formulation presented in the previous chapter. Our computation is restricted to a cuboidal domain Ω of sides L_1, L_2 and L_3. We generate a uniform finite-difference grid with spacing h such that $L_1 = n_1 h$, $L_2 = n_2 h$ and $L_3 = n_3 h$, where n_1, n_2 and n_3 are natural numbers. The grid points are indexed by (i, j, k), where $i = 1, 2, \ldots, n_1$, $j = 1, 2, \ldots, n_2$ and $k = 1, 2, \ldots, n_3$. The Laplacian of any function $f(\mathbf{x})$ at the grid point (i, j, k) can be approximated using higher-order finite-differences [40]

$$\begin{aligned} \nabla^2 f\big|^{(i,j,k)} &\approx \sum_{p=0}^{N} w_p \Big(f^{(i+p,j,k)} + f^{(i-p,j,k)} + f^{(i,j+p,k)} \\ &+ f^{(i,j-p,k)} + f^{(i,j,k+p)} + f^{(i,j,k-p)} \Big), \end{aligned} \tag{49}$$

where $f^{(i,j,k)}$ represents the value of the function $f(\mathbf{x})$ at the grid point (i, j, k). The weights w_p are given by [43, 36, 57]

$$\begin{aligned} w_0 &= -\frac{1}{h^2} \sum_{q=1}^{N} \frac{1}{q^2}, \\ w_p &= \frac{2(-1)^{p+1}}{h^2 p^2} \frac{(N!)^2}{(N-p)!(N+p)!}, \; p = 1, 2, \ldots, N. \end{aligned} \tag{50}$$

Similarly, the gradient at the grid point (i, j, k) can be approximated using higher-order finite-differences

$$\begin{aligned} \nabla f\big|^{(i,j,k)} &\approx \sum_{p=1}^{N} \tilde{w}_p \Big((f^{(i+p,j,k)} - f^{(i-p,j,k)}) \hat{\mathbf{e}}_1 + (f^{(i,j+p,k)} - f^{(i,j-p,k)}) \hat{\mathbf{e}}_2 \\ &+ (f^{(i,j,k+p)} - f^{(i,j,k-p)}) \hat{\mathbf{e}}_3 \Big), \end{aligned} \tag{51}$$

where $\hat{\mathbf{e}}_1$, $\hat{\mathbf{e}}_2$ and $\hat{\mathbf{e}}_3$ represent unit vectors along the edges of the cuboidal domain Ω. The weights $\tilde{w}_p$ are given by [43, 36, 57]

$$\tilde{w}_p = \frac{(-1)^{p+1}}{hp} \frac{(N!)^2}{(N-p)!(N+p)!}\,,\ p = 1, 2, \ldots, N. \tag{52}$$

These finite-difference expressions for the Laplacian and gradient represent $2N$ order accurate approximations, i.e. error is $\mathcal{O}(h^{2N})$. While performing spatial integrations, we assume that the function $f(\mathbf{x})$ is constant in a cube of side h around each grid point i.e.

$$\int_{\Omega} f(\mathbf{x})\,\mathrm{d}\mathbf{x} \approx h^3 \sum_{i=1}^{n_1} \sum_{j=1}^{n_2} \sum_{k=1}^{n_3} f^{(i,j,k)}. \tag{53}$$

Periodic boundary conditions on Ω is enforced by employing the following strategy. In the finite-difference representations of the Laplacian and gradient as presented in Eqns. 49 and 51 respectively, we map any index that does not correspond to a node in the finite-difference grid to its periodic image within Ω.

We start with precomputed radially-symmetric and compactly-supported isolated-atom electron densities for each type of atom. These isolated-atom electron densities are then superimposed for the initial configuration of the nuclei, followed by scaling the resulting electron density such that the constraint on the total number of electrons is satisfied. We take the pointwise square-root of the electron density so obtained as the starting guess $u_0^{(i,j,k)}$. During the aforedescribed calculation, we only visit atoms whose isolated-atom electron densities have non-zero overlap with Ω. Similarly, for every new configuration of atoms encountered during the geometry optimization, we calculate the charge density of the nuclei using the relations

$$b^{(i,j,k)} = \sum_J b_J^{(i,j,k)}\,, \quad b_J^{(i,j,k)} = -\frac{1}{4\pi} \nabla^2 V_J \big|^{(i,j,k)}\,, \tag{54}$$

where the summation reduces to all atoms whose charge density has non-zero overlap with Ω. The localized nature of the above operations ensures that the evaluation of $u_0^{(i,j,k)}$ and $b^{(i,j,k)}$ scales linearly with the number of atoms.

We solve the variational problem in Eqn. 43 using a conjugate gradient method that was originally developed for DFT [58, 47] and later adopted in simplified form for OF-DFT [60, 35, 29]. Specifically, the Polak-Ribiere update [52] with Brent's method [50] for the line-search has been utilized. We refer the reader to Appendix C for further details on the algorithm implemented in this work. For every update in the square-root electron density, we solve the Poisson equation in Eqn. 36 under periodic boundary conditions using the Generalized minimal residual method (GMRES) [51] with the block-Jacobi preconditioner [25]. Since the solution so obtained is accurate to within an indeterminate constant, we enforce the condition $\int_\Omega \phi(\mathbf{x})\,\mathrm{d}\mathbf{x} = 0$ for definiteness. In every subsequent Poisson equation encountered, we use the previous solution as starting guess. For the complex-valued Helmholtz equations in Eqns. 22 and 23, we first separate out each equation into its real and imaginary parts. Then we solve the resulting coupled equations simultaneously under periodic boundary conditions using the GMRES method with block-Jacobi preconditioners. In every iteration of the fixed-point method, we use the solution of the Helmholtz equations from the previous iteration as the starting guess. We accelerate the convergence of the fixed-point iteration by utilizing Anderson mixing [1], details of which can be found in Appendix D.

Once the electronic ground-state square-root electron density has been determined, the energy and forces are evaluated using Eqns. 46 and 47 respectively. While doing so, we restrict the summation over the periodic images to atoms whose charge density has non-zero overlap with Ω. We solve for the equilibrium configuration of the atoms by using the conjugate gradient method with the Polak-Ribiere update and secant line search [52]. We have developed a parallel implementation of the proposed approach using the Portable, Extensible Toolkit for scientific computations (PETSc) [2, 3] suite of data structures and routines. Within PETSc, we have utilized distributed arrays with the star-type stencil option. The communication between the

processors is handled via the Message Passing Interface (MPI) [27].

CHAPTER V

EXAMPLES AND RESULTS

In this Chapter, we validate the proposed formulation and higher-order finite-difference implementation of periodic OF-DFT through selected examples. We shall refer to the implementation developed in this work as RS-FD, which is an acronym for Real-Space Finite-Differences. In all the simulations, we employ the Goodwin-Needs-Heine pseudopotential [26] and wherever applicable, we compare our results with the plane-wave code PROFESS [29, 34]. We choose $\lambda = \frac{1}{5}$ for the TFW functional, and $\lambda = 1$, $L = 2$, $R = 4$, $\alpha = \frac{5}{6} + \frac{\sqrt{5}}{6}$ and $\beta = \frac{5}{6} - \frac{\sqrt{5}}{6}$ for the WGC functional. Within PROFESS, we utilize a plane-wave energy cutoff of $E_{cut} = 1200$ eV, which results in energies and forces that are converged to within 1×10^{-6} eV/atom and 6×10^{-4} eV/Bohr respectively. Unless specified otherwise, we use sixth-order accurate finite-differences and a mesh size $h = 0.5$ Bohr within RS-FD, which results in energies and forces that are converged to within 0.006 eV/atom and 0.007 eV/Bohr respectively.

5.1 Convergence of energy with spatial discretization

We start by verifying convergence of the computed energy with respect to the finite-difference approximation. We choose a FCC unit cell of Aluminum with lattice constant $a = 8.0$ Bohr as the representative example. We evaluate the energy of this system as a function of mesh size h for the TFW and WGC kinetic energy functionals while utilizing second and sixth order accurate finite-differences. Anticipating polynomial convergence with respect to h, we fit the data to a power law of the form

$$\mathcal{E} = C_{\mathcal{E}} h^p + \mathcal{E}_c, \tag{55}$$

where the prefactor $C_{\mathcal{E}}$, convergence rate p, and estimate of the $h \rightarrow 0$ energy $\mathcal{E}_c$ are the parameters to be fitted. We present the results so obtained in Table 1, and verify the quality of the fit in Fig. 2. In this plot, we have utilized $\mathcal{E}_c$ as the reference value and $h_0 = 0.08$ Bohr to normalize the mesh size.

When the electronic kinetic energy is modeled using the TFW functional, sixth-order accurate finite-differences is able to achieve significantly higher rates of convergence compared to second-order finite-differences. In fact, the extrapolated value of $\mathcal{E}_c = -60.2210$ eV/atom for sixth-order finite-differences is in good agreement with energy $\mathcal{E} = -60.2207$ eV/atom obtained by PROFESS. However, the extrapolated value of $\mathcal{E}_c = -60.2535$ for second-order finite-differences is appreciably different. This indicates that even finer meshes are required for an accurate extrapolation. Irrespective of this issue, it can be concluded from Fig. 2 that second-order finite-differences will be prohibitively expensive for obtaining the chemical accuracies desired in OF-DFT calculations. Notably, higher-order finite-differences are able to perform equally well when the WGC kinetic energy functional is employed. In particular, sixth-order finite-differences is able to achieve a convergence rate of $p = 4.96$ with respect to the mesh-size. Further, the predicted value of $\mathcal{E}_c = -58.2671$ eV/atom is in good agreement with the energy $\mathcal{E} = -58.2658$ eV/atom calculated by PROFESS.

Overall, we conclude that higher-order finite-differences are necessary for performing accurate and efficient electronic structure calculations based on OF-DFT. Indeed, larger convergence rates may be possible as the order of the finite-difference approximation is increased. However, this comes at the price of increased computational cost per iteration due to the reduced locality of the discretized operators and larger inter-processor communication. We have found sixth-order finite-differences to be an efficient choice, which is in agreement with our previous conclusions for the non-periodic setting [57]. In view of this, we will employ sixth-order finite-differences for the remaining simulations in this work.

Table 1: Parameters for the convergence in energy obtained by fitting Eqn. 55. The system under consideration is a single FCC unit cell of Aluminum with lattice constant $a = 8.0$ Bohr.

Kinetic energy functional	FD order	$C_{\mathcal{E}}$	p	$\mathcal{E}_c$ (eV/atom)
TFW	Second	$+0.1557$	1.01	-60.2535
TFW	Sixth	-0.2121	5.46	-60.2210
WGC	Sixth	-0.1206	4.96	-58.2671

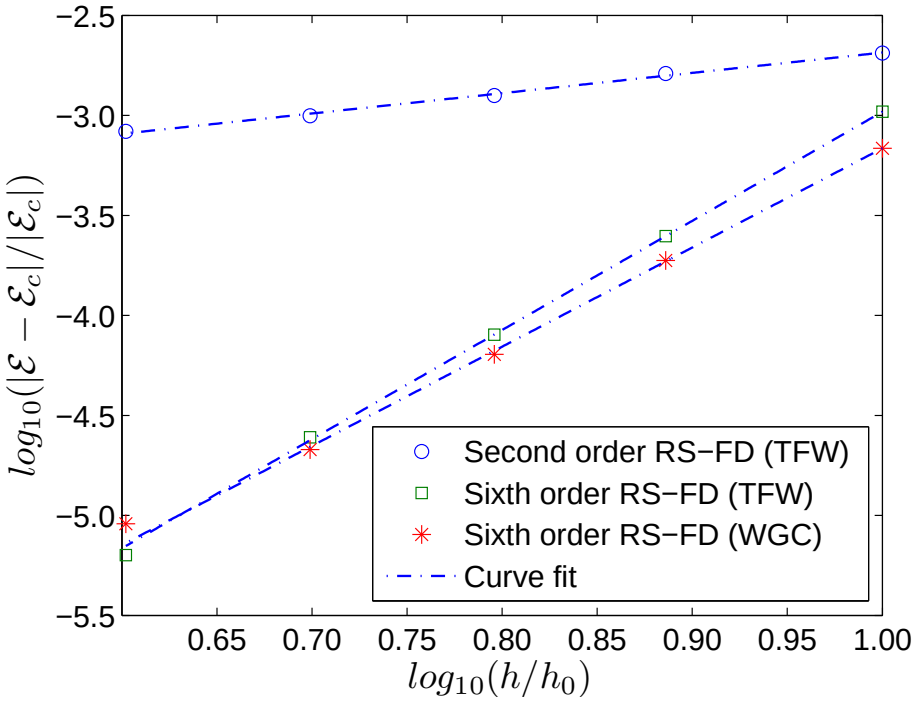

Figure 2: Convergence in the energy as a function of mesh size for a single FCC unit cell of Aluminum with lattice constant $a = 8.0$ Bohr.

5.2 Convergence of forces with spatial discretization

In this section, we verify the convergence of the forces with respect to the finite-difference discretization. Specifically, we choose an Aluminum dimer with bond length of $R = 8.0$ Bohr as the representative example. We employ the TFW kinetic energy functional, choose a domain such that the minimum distance between any atom and the boundary is 12.0 Bohr, and use sixth-order accurate finite-differences. We calculate the interatomic force f for different mesh sizes h and fit the data to a power law of the form

$$f = C_f h^q + f_c, \tag{56}$$

where the prefactor C_f, convergence rate q, and estimate of the $h \to 0$ force f_c are the parameters to be fitted. We present the results so obtained in Table 2, which demonstrates that the error in the force scales as $\mathcal{O}(h^5)$. Additionally, the value of $f_c = 0.1220$ eV/Bohr is in good agreement with the force of $f = 0.1224$ eV/Bohr calculated by PROFESS. Overall, from this and other examples which are not presented here, we conclude that higher-order finite-differences are capable of achieving relatively large convergence rates in both the energies and the forces. This feature along with the notable simplicity in implementation makes them very attractive for performing electronic structure calculations based on OF-DFT.

Table 2: Parameters for the convergence in the interatomic force obtained by fitting Eqn. 56. The system under consideration is an Aluminum dimer with bond length $R = 8.0$ Bohr.

Kinetic energy functional	FD order	C_f	q	f_c (eV/Bohr)
TFW	Sixth	0.0147	4.99	0.1220

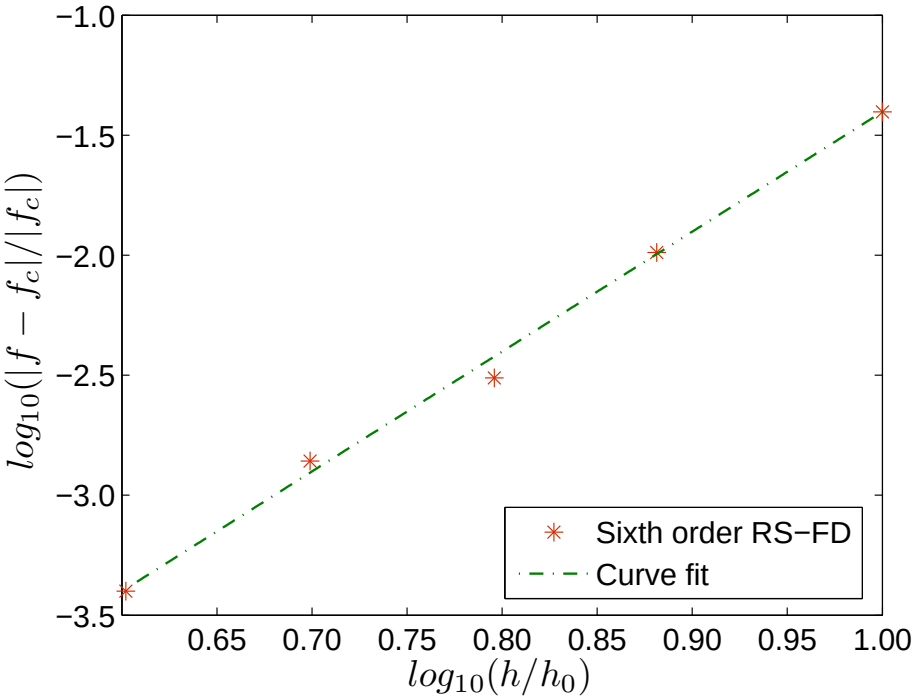

Figure 3: Convergence in the interatomic force as a function of mesh size for an Aluminum dimer with bond length $R = 8.0$ Bohr.

5.3 Convergence of the fixed-point method

In this section, we demonstrate convergence of the fixed-point method for simulations involving the WGC kinetic energy functional. We choose two examples, namely a supercell consisting of $6 \times 6 \times 6$ FCC Aluminum unit cells with and without a vacancy. We utilize a lattice constant of $a = 7.50$ Bohr, mesh-size of $h = 0.5$ Bohr, and history of three iterations for Anderson mixing,which we have found to work well. In Fig. 4, we present the error in the fixed-point iteration for the two aforementioned examples. Specifically, we compare the peformance of Anderson mixing with the standard fixed-point iteration, i.e. without mixing. We observe that Anderson mixing significantly accelerates the convergence of the fixed-point iteration, with the mixing parameter $\zeta = 1$ demonstrating the best performance. We have found these results to be representative of other simulations utilizing the WGC kinetic energy functional. In view of this, we will utilize Anderson mixing with $\zeta = 1$ for the remaining simulations in this work. It is worth noting that using a larger number of previous iterates in Anderson mixing has the potential to further reduce the number of fixed-point iterations required for convergence.

In this work, we have presented a fixed-point iteration with respect to $V_{LR}(\mathbf{x})$ for simulations involving linear-response kinetic energy functionals. However, it is also possible to develop an analogous fixed-point iteration with respect to $u(\mathbf{x})$. In Table 3, we compare the performances of the fixed-point iterations with respect to $u(\mathbf{x})$ and $V_{LR}(\mathbf{x})$ for a couple of examples employing the WGC kinetic energy functional. In both cases, we have employed Anderson mixing with a history of three iterations. We can see that the relative performance of each of the fixed-point choices is system dependent. However, we have found the fixed-point iteration with respect to $V_{LR}(\mathbf{x})$ to be significantly more robust than the one with respect to $u(\mathbf{x})$. Therefore, we have chosen the fixed-point iteration with respect to $V_{LR}(\mathbf{x})$ for all simulations involving the WGC kinetic energy functional.

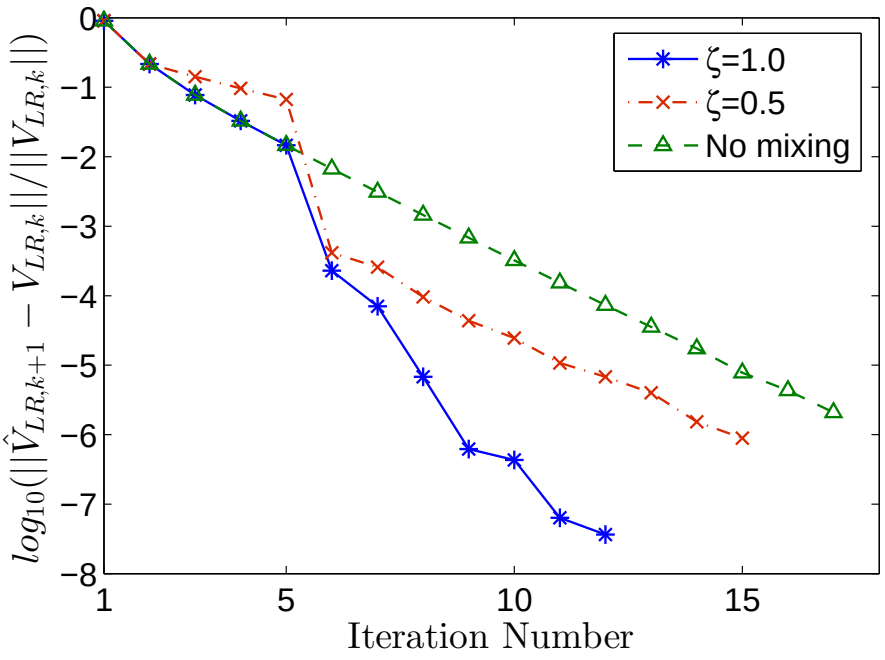

(a) Perfect crystal

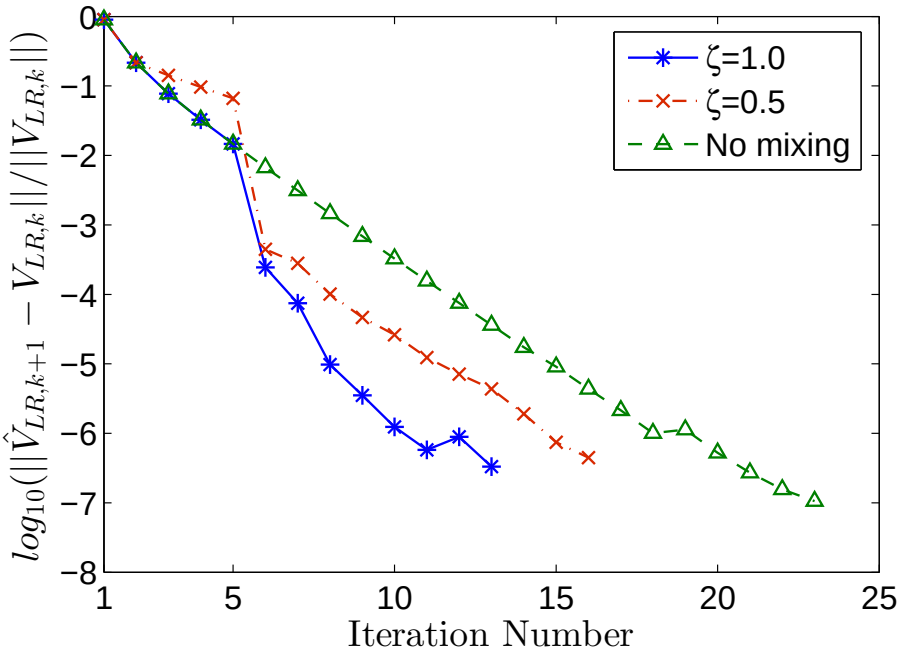

(b) Vacancy

Figure 4: Convergence of the fixed-point iteration for a supercell consisting of $6 \times 6 \times 6$ FCC Aluminum unit cells with lattice constant of $a = 7.50$ Bohr. The atoms are held fixed in their original lattice positions.

Table 3: Comparison of the performances for different fixed-point iterations accelerated by Anderson mixing. The atoms are held fixed in their original lattice positions.

System	Fixed-point iterations for u	Fixed-point iterations for V_{LR}
$3 \times 3 \times 3$ FCC unit cells perfect crystal	15	22
$6 \times 6 \times 6$ FCC unit cells with a vacancy	29	18

5.4 Examples

5.4.1 Aluminum clusters

First, we study Aluminum clusters consisting of $M_a = 14$, 172, 666, 1688 and 3430 atoms that are arranged as $1\times1\times1$, $3\times3\times3$, $5\times5\times5$, $7\times7\times7$ and $9\times9\times9$ FCC unit cells of Aluminum respectively. The atoms are held fixed, with the lattice constants chosen to minimize the energy [57]. Further, the size of the cubical domains are such that the minimum distance of any atom to the boundary is 12 Bohr. In order to avoid the vacuum resulting divergences encountered when using the WGC functional, we employ the TFW kinetic energy functional. In Tables 4 and 5, we compare the energies and forces as computed by RS-FD with PROFESS. It is clear that there is very good agreement in the energies and forces. In particular, the maximum difference in the energy is 0.005 eV/atom with the difference in the forces being 0.00160 eV/Bohr (l_1 norm), 0.00013 eV/Bohr (l_2 norm) and 0.00683 eV/Bohr (*sup* norm).

Table 4: Energy of $m \times m \times m$ FCC Aluminum unit cell clusters, where $m = 1$, 3, 5, 7 and 9.

FCC Aluminum unit cells	No. of atoms (M_a)	a_e (Bohr)	$\mathcal{E}$ (eV/atom) RS-FD	$\mathcal{E}$ (eV/atom) PROFESS
$1 \times 1 \times 1$	14	7.73	-59.246	-59.241
$3 \times 3 \times 3$	172	7.89	-59.813	-59.808
$5 \times 5 \times 5$	666	7.93	-59.965	-59.960
$7 \times 7 \times 7$	1688	7.95	-60.035	-60.030
$9 \times 9 \times 9$	3430	7.96	-60.075	-60.071

Table 5: Comparison of forces with PROFESS for $m \times m \times m$ FCC Aluminum unit cell clusters, where $m = 1$, 3, 5, 7 and 9.

FCC Aluminum unit cells	l_1 norm/$(3M_a)$ (eV/Bohr)	l_2 norm/$(3M_a)$ (eV/Bohr)	*sup* norm (eV/Bohr)
$1 \times 1 \times 1$	0.00070	0.00013	0.00133
$3 \times 3 \times 3$	0.00082	0.00004	0.00211
$5 \times 5 \times 5$	0.00160	0.00004	0.00409
$7 \times 7 \times 7$	0.00038	0.00001	0.00217
$9 \times 9 \times 9$	0.00158	0.00002	0.00683

5.4.2 Aluminum crystal

Next, we calculate the bulk properties of FCC Aluminum for the TFW and WGC kinetic energy functionals using a supercell consisting of $5 \times 5 \times 5$ FCC Aluminum unit cells ($M_a = 600$). We start by calculating the energy $\mathcal{E}$ using RS-FD and PROFESS for various lattice constants a, the results of which are presented in Fig. 5. Next, we employ a cubic fit to the data to determine the equilibrium lattice constant a_e and the bulk modulus [17]

$$B = \frac{4}{9a_e} \frac{\partial^2 \mathcal{E}}{\partial a^2}\bigg|_{a_e}. \tag{57}$$

It is evident from the results in Table 6 that the predictions of RS-FD are in very good agreement with PROFESS. In fact, the equilibrium lattice constants are identical to within 0.01 Bohr for both the TFW and WGC functionals. The difference in the energy for the TFW and WGC functionals is 0.005 eV/atom and 0.003 eV/atom respectively, with the difference in the bulk modulus being 0.006 GPa and 0.859 GPa respectively. The slight difference in bulk modulus for the WGC functional can be attributed to the fact that RS-FD approximates the kernels $K_{mn}(|\mathbf{x} - \mathbf{x}'|)$ in Fourier space using rational functions. Indeed, we anticipate that using a larger number of rational functions to approximate $K_{mn}(|\mathbf{x} - \mathbf{x}'|)$ will further improve the agreement between RS-FD and PROFESS.

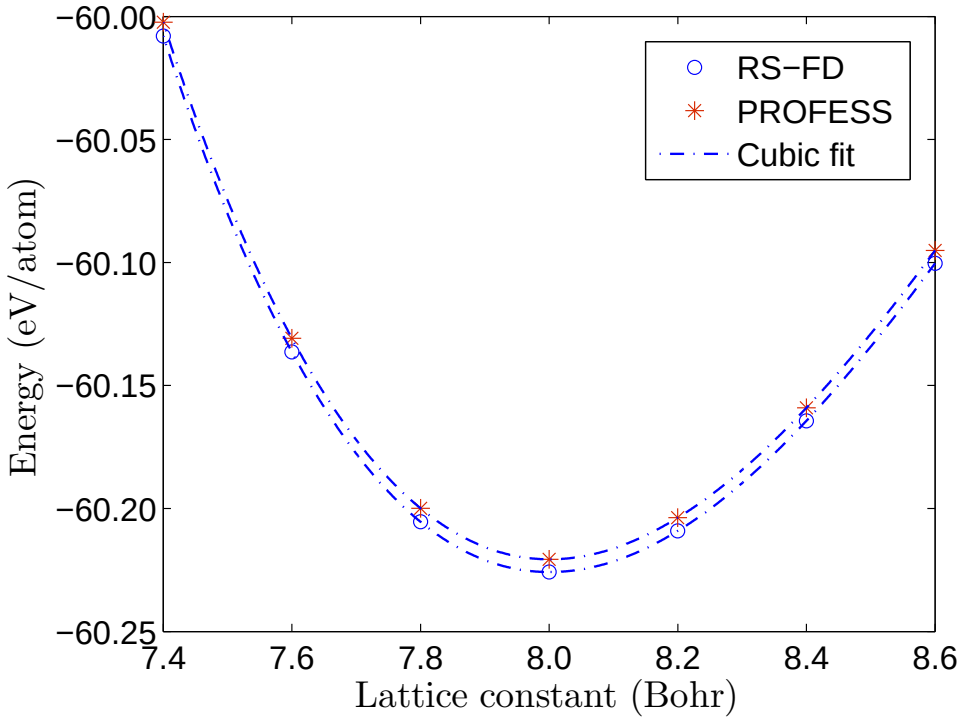

(a) TFW

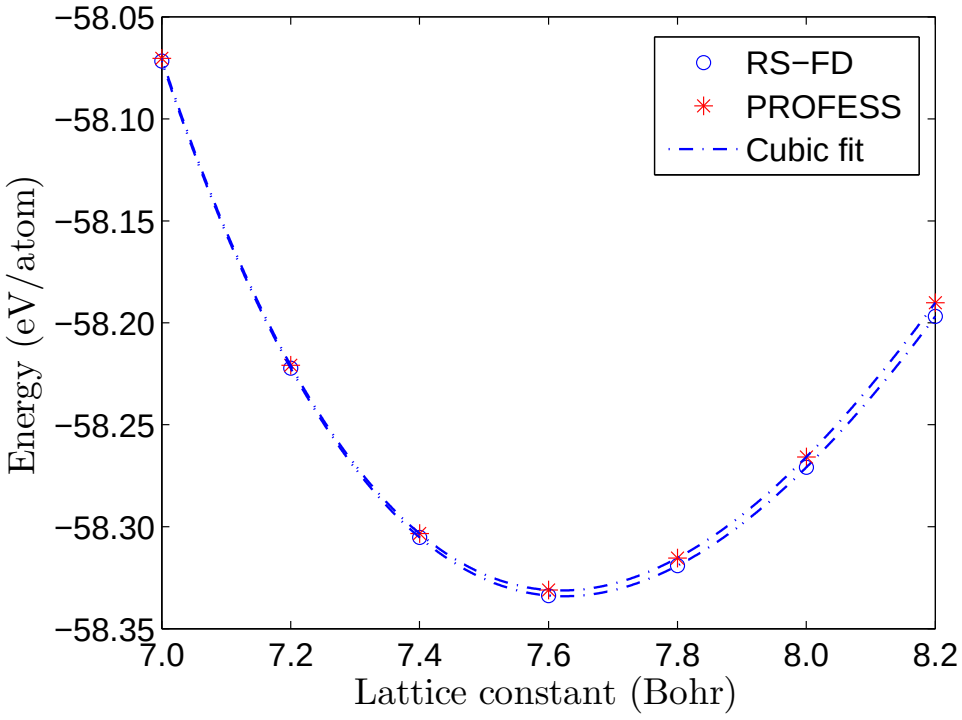

(b) WGC

Figure 5: Variation of energy with lattice constant for FCC Aluminum.

Table 6: Bulk properties of FCC Aluminum.

Kinetic energy functional	Method	$\mathcal{E}$ (eV/atom)	a_e (Bohr)	B (GPa)
TFW	RS-FD	-60.226	8.00	57.3
	PROFESS	-60.221	8.00	57.3
WGC	RS-FD	-58.335	7.62	68.1
	PROFESS	-58.332	7.62	68.9

5.4.3 Vacancy formation energy in Aluminum

Finally, we calculate the vacancy formation energy in stress-free FCC Aluminum. We consider a supercell consisting $6 \times 6 \times 6$ FCC Aluminum unit cells ($M_a = 864$), and remove an atom from the center to create a vacancy. We calculate the vacancy formation energy $\mathcal{E}_{vf}$ using the relation [17, 23]

$$\mathcal{E}_{vf} = \mathcal{E}\left(M_a - 1, 1, \frac{M_a - 1}{M_a}\Omega\right) - \left(\frac{M_a - 1}{M_a}\right)\mathcal{E}(M_a, 0, \Omega)\,, \tag{58}$$

where $\mathcal{E}(M_a, n, \Omega)$ is used to denote the energy of a periodic cell Ω with M_a occupied lattice sites and n vacancies. We present the results so obtained in Table 7, and plot the electron density contours on the mid-plane for the TFW and WGC kinetic energy functionals in Figs. 6 and 7 respectively. We observe that the computed vacancy formation energies are in good agreement with PROFESS. In fact, the relaxed vacancy formation energies are identical to within 0.01 eV and 0.02 eV when using the TFW and WGC functionals respectively. As discussed in the previous section, the larger discrepancy in WGC can be attributed to the approximate kernels $K_{mn}(|\mathbf{x}-\mathbf{x}'|)$ employed in RS-FD. From the final relaxed configuration of the atoms, we find that the average l_2 norm of the difference in the positions of the nuclei obtained by RS-FD and PROFESS to be 4.6×10^{-5} Bohr for TFW functional case and 7.0×10^{-6} Bohr for WGC functional.

Table 7: Vacancy formation energy in stress-free FCC Aluminum

Kinetic energy functional	Method	a_e (Bohr)	$\mathcal{E}_{vf}$ (unrelaxed) (eV)	$\mathcal{E}_{vf}$ (relaxed) (eV)
TFW	RS-FD	8.00	0.87	0.83
	PROFESS	8.00	0.87	0.83
WGC	RS-FD	7.62	0.60	0.49
	PROFESS	7.62	0.59	0.47

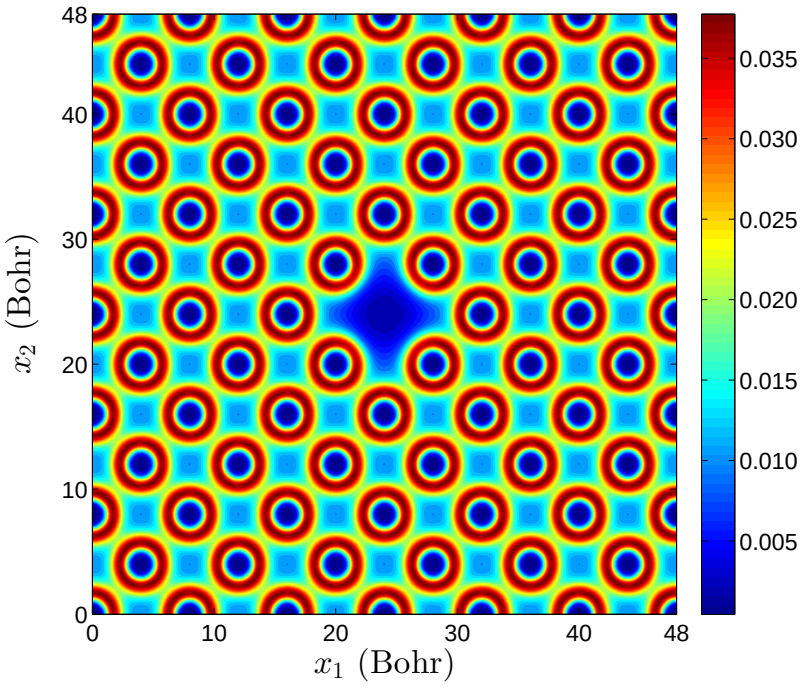

(a) Unrelaxed vacancy

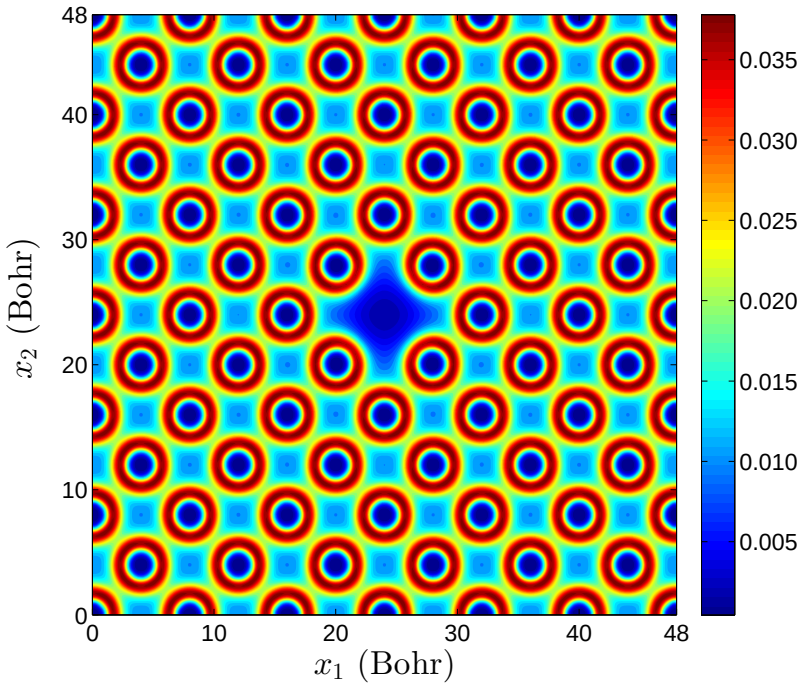

(b) Relaxed vacancy

Figure 6: Electron density contours on the mid-plane of FCC Aluminum with a vacancy. The TFW kinetic energy functional has been employed.

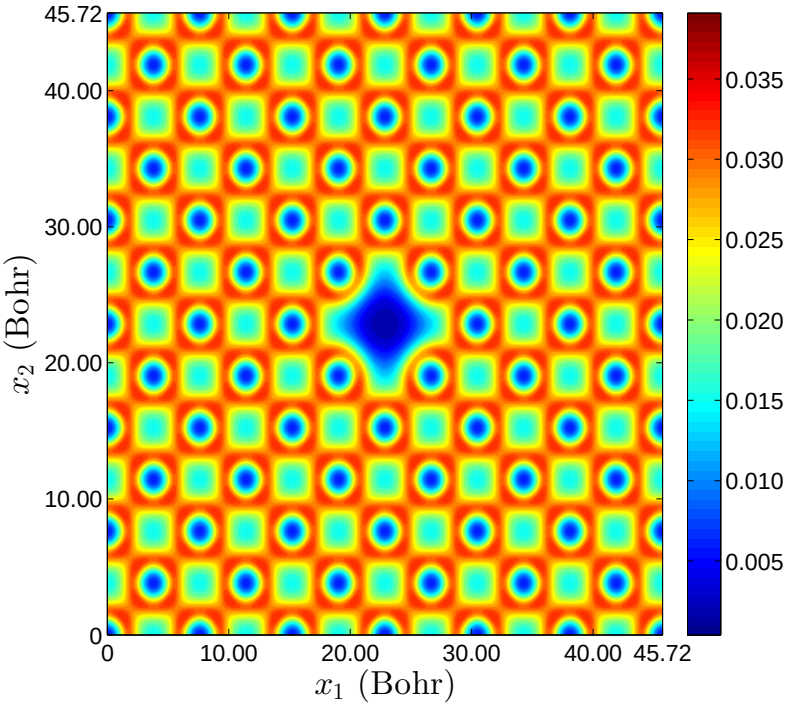

(a) Unrelaxed vacancy

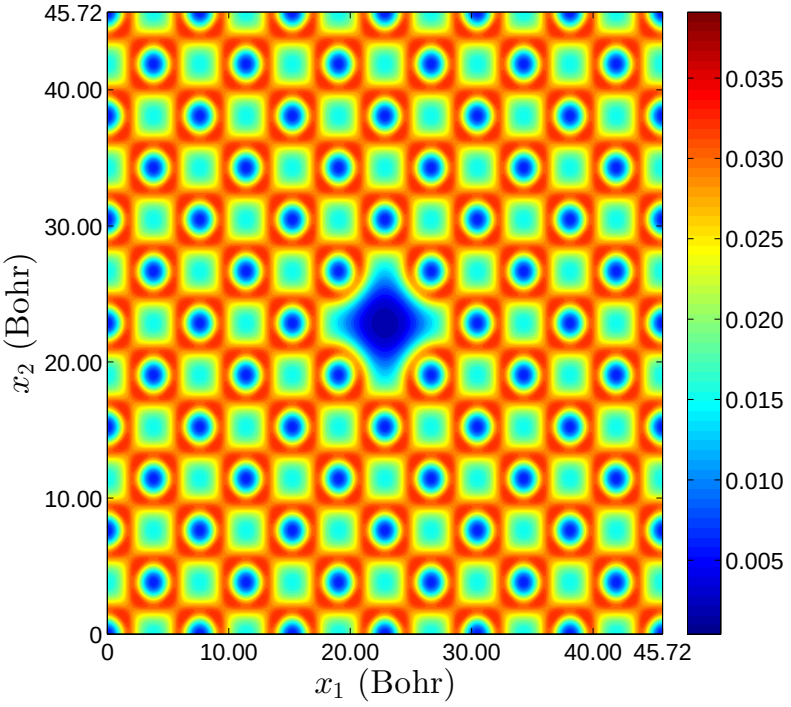

(b) Relaxed vacancy

Figure 7: Electron density contours on the mid-plane of FCC Aluminum with a vacancy. The WGC kinetic energy functional has been employed.

CHAPTER VI

CONCLUSION

This thesis presents a real-space formulation and higher-order finite-difference implementation of periodic Orbital-free Density Functional Theory (OF-DFT). Specifically, utilizing a local reformulation of the electrostatics and kernel energy/potential, a generalized framework for performing OF-DFT simulations that is able to accommodate the different variants of the electronic kinetic energy has been developed. In particular, for linear-response kinetic energy functionals, we have developed a fixed-point technique that is similar in spirit to the self-consistent field (SCF) method employed in DFT calculations. We have also developed a parallel finite-difference implementation of this formulation, using which we have demonstrated that higher-order finite-differences can achieve relatively large convergence rates with respect to mesh-size in both the energies and forces. Additionally, we have established that the fixed-point iteration converges rapidly, and that it can be further accelerated using extrapolation schemes like Anderson mixing. We have verified the accuracy of our results by comparing the energies and forces with plane-wave methods for selected examples.

Overall, we conclude that higher-order finite-differences are an attractive choice for performing electronic structure calculations based on OF-DFT. This is due to their simplicity, potential for scalability to massively-parallel distributed-memory computer architectures, and ability to efficiently achieve chemical accuracies desired in electronic structure calculations. One limitation of the developed implementation is the lack of an effective real-space preconditioner, which is currently being pursued. Finally, we note that extending the current work to finite-temperatures and therefore enabling molecular dynamics simulations is a worthy subject of future research.

APPENDIX A

COEFFICIENTS IN THE HELMHOLTZ EQUATIONS FOR THE WGC KINETIC ENERGY FUNCTIONAL

The coefficients P_{mnr} and Q_{mnr} arising in the Helmholtz equations given in Eqns. 22 and 23 are determined by fitting the kernels $K_{mn}(|\mathbf{x}-\mathbf{x}'|)$ in Fourier space using rational functions [12]. In Table 8, we present the values for the WGC functional when a fourth-order expansion ($R=4$) is employed. The coefficients satisfy the relations $P_{mnr}=P_{nmr}$ and $Q_{mnr}=Q_{nmr}$, with $P_{mn2}=P^*_{mn1}$, $Q_{mn2}=Q^*_{mn1}$, $P_{mn4}=P^*_{mn3}$ and $Q_{mn4}=Q^*_{mn3}$. Here, the superscript $*$ denotes the complex conjugate.

Table 8: Coefficients in the Helmholtz equations (Eqns. 22 and 23) for the WGC kinetic energy functional [12].

Coefficients	$r=1$	$r=3$
P_{00r}	$+0.108403+i0.079657$	$-0.908403+i0.439708$
Q_{00r}	$-0.470923-i0.465392$	$+0.066051-i0.259678$
P_{10r}	$-0.030515+i0.015027$	$+0.028915-i0.008817$
Q_{10r}	$-0.597793-i0.294130$	$-0.087917-i0.164937$
P_{20r}	$+0.008907-i0.032841$	$-0.034974+i0.009116$
Q_{20r}	$-0.537986-i0.233840$	$-0.041565-i0.196662$
P_{11r}	$+0.012423-i0.034421$	$-0.031907+i0.007392$
Q_{11r}	$-0.511699-i0.0266195$	$-0.034031-i0.188927$

APPENDIX B

ELECTROSTATIC CORRECTION FOR OVERLAPPING CHARGE DENSITY OF NUCLEI

In the local electrostatic reformulation presented in Section 3.2, the repulsive energy can be expressed as

$$\mathcal{E}_{\text{zz}}(\mathbf{R}) = \frac{1}{2}\int_{\Omega}\int_{\mathbb{R}^3} \frac{b(\mathbf{x},\mathbf{R})b(\mathbf{x}',\mathbf{R})}{|\mathbf{x}-\mathbf{x}'|}\,\mathrm{d}\mathbf{x}'\,\mathrm{d}\mathbf{x} - \frac{1}{2}\sum_{J}\int_{\Omega} b_J(\mathbf{x},\mathbf{R}_J)V_J(\mathbf{x},\mathbf{R}_J)\,\mathrm{d}\mathbf{x}\,, \quad (59)$$

where the second term accounts for the self energy of the nuclei. Using Eqn. 28, we arrive at

$$\begin{aligned}\mathcal{E}_{\text{zz}}(\mathbf{R}) &= \frac{1}{2}\sum_{I}\sum_{J}\int_{\Omega} b_I(\mathbf{x},\mathbf{R}_I)V_J(\mathbf{x},\mathbf{R}_J)\,\mathrm{d}\mathbf{x} - \frac{1}{2}\sum_{J}\int_{\Omega} b_J(\mathbf{x},\mathbf{R}_J)V_J(\mathbf{x},\mathbf{R}_J)\,\mathrm{d}\mathbf{x} \\ &= \frac{1}{2}\sum_{I}\sum_{\substack{J\\J\neq I}}\int_{\Omega} b_I(\mathbf{x},\mathbf{R}_I)V_J(\mathbf{x},\mathbf{R}_J)\,\mathrm{d}\mathbf{x}\,. \end{aligned} \quad (60)$$

Above, the summations over I and J extends to all atoms in $\mathbb{R}^3$. If the charge density of the nuclei do not overlap, Eqn. 60 can be rewritten as

$$\begin{aligned}\mathcal{E}_{\text{zz}}(\mathbf{R}) &= \frac{1}{2}\sum_{I}\sum_{\substack{J\\J\neq I}} Z_J\int_{\Omega}\frac{b_I(\mathbf{x},\mathbf{R}_I)}{|\mathbf{x}-\mathbf{R}_J|}\,\mathrm{d}\mathbf{x} = \frac{1}{2}\sum_{I}\sum_{\substack{J_\Omega\\J_\Omega\neq I}} Z_{J_\Omega}V_I(\mathbf{R}_{J_\Omega},\mathbf{R}_I) \\ &= \frac{1}{2}\sum_{I}\sum_{\substack{J_\Omega\\J_\Omega\neq I}}\frac{Z_I Z_{J_\Omega}}{|\mathbf{R}_I-\mathbf{R}_{J_\Omega}|}\,, \end{aligned} \quad (61)$$

which is exactly the expression given in Eqn. 14 for the repulsive energy prior to reformulation. However, the use of relatively 'soft' pseudopotentials — which are attractive because of the significant reduction in the number of basis functions required for convergence — can frequently result in overlapping charge density of the nuclei. In this situation, the repulsive energy and the forces on the nuclei will be inaccurately calculated. Below, we present a technique to correct for these errors.

We start by generating a 'reference' charge density

$$\tilde{b}(\mathbf{x},\mathbf{R}) = \sum_J \tilde{b}_J(\mathbf{x},\mathbf{R}_J)\,, \tag{62}$$

which is the superposition of spherically symmetric and compactly supported 'reference' charge densities $\tilde{b}_J(\mathbf{x},\mathbf{R}_J)$. These nuclei-centered charge densities satisfy the relations

$$\int_{\mathbb{R}^3} \tilde{b}_J(\mathbf{x},\mathbf{R}_J)\,\mathrm{d}\mathbf{x} = Z_J\,, \quad \int_\Omega \tilde{b}(\mathbf{x},\mathbf{R})\,,\mathrm{d}\mathbf{x} = N_e\,. \tag{63}$$

Thereafter, the correction to the repulsive energy can be expressed as

$$\begin{aligned}\mathcal{E}_c^*(\mathbf{R}) &= \frac{1}{2}\int_\Omega\int_{\mathbb{R}^3} \frac{\tilde{b}(\mathbf{x},\mathbf{R})\tilde{b}(\mathbf{x}',\mathbf{R})}{|\mathbf{x}-\mathbf{x}'|}\,\mathrm{d}\mathbf{x}'\,\mathrm{d}\mathbf{x} - \frac{1}{2}\int_\Omega\int_{\mathbb{R}^3} \frac{b(\mathbf{x},\mathbf{R})b(\mathbf{x}',\mathbf{R})}{|\mathbf{x}-\mathbf{x}'|}\,\mathrm{d}\mathbf{x}'\,\mathrm{d}\mathbf{x} \\ &\quad -\frac{1}{2}\sum_J\int_\Omega \tilde{b}_J(\mathbf{x},\mathbf{R}_J)\tilde{V}_J(\mathbf{x},\mathbf{R}_J)\,\mathrm{d}\mathbf{x} + \frac{1}{2}\sum_J\int_\Omega b_J(\mathbf{x},\mathbf{R}_J)V_J(\mathbf{x},\mathbf{R}_J)\,\mathrm{d}\mathbf{x}\end{aligned} \tag{64}$$

A direct computation of this energy correction will scale quadratically with respect to the number of atoms. In order to enable linear-scaling, we rewrite Eqn. 64 as

$$\begin{aligned}\mathcal{E}_c^*(\mathbf{R}) &= \frac{1}{2}\int_\Omega \Big(\tilde{b}(\mathbf{x},\mathbf{R}) + b(\mathbf{x},\mathbf{R})\Big)\,V_c(\mathbf{x},\mathbf{R})\,\mathrm{d}\mathbf{x} + \frac{1}{2}\sum_J\int_\Omega b_J(\mathbf{x},\mathbf{R}_J)V_J(\mathbf{x},\mathbf{R}_J)\,\mathrm{d}\mathbf{x} \\ &\quad -\frac{1}{2}\sum_J\int_\Omega \tilde{b}_J(\mathbf{x},\mathbf{R}_J)\tilde{V}_J(\mathbf{x},\mathbf{R}_J)\,\mathrm{d}\mathbf{x}\,,\end{aligned} \tag{65}$$

where $V_c(\mathbf{x},\mathbf{R})$ is the solution to the Poisson equation

$$\frac{-1}{4\pi}\nabla^2 V_c(\mathbf{x},\mathbf{R}) = \tilde{b}(\mathbf{x},\mathbf{R}) - b(\mathbf{x},\mathbf{R}) \tag{66}$$

with periodic boundary conditions. The potential $V_c(\mathbf{x},\mathbf{R})$ so calculated is accurate to within a constant, which can be determined by evaluating $\sum_J(V_J(\mathbf{x},\mathbf{R}_J) - \tilde{V}_J(\mathbf{x},\mathbf{R}_J))$ at any point in space.

The correction to the forces on the nuclei

$$\mathbf{f}_J^c = -\frac{\partial \mathcal{E}_c^*(\mathbf{R})}{\partial \mathbf{R}_J} \tag{67}$$

can be represented as

$$\begin{aligned}
\mathbf{f}_J^c &= -\frac{1}{2}\sum_{J'}\int_\Omega \left[\frac{\partial \tilde{b}_{J'}(\mathbf{x},\mathbf{R}_{J'})}{\partial \mathbf{R}_{J'}}\left(V_c(\mathbf{x},\mathbf{R}) - \tilde{V}_{J'}(\mathbf{x},\mathbf{R}_{J'})\right)\right. \\
&\quad + \frac{\partial b_{J'}(\mathbf{x},\mathbf{R}_{J'})}{\partial \mathbf{R}_{J'}}\left(V_c(\mathbf{x},\mathbf{R}) + V_{J'}(\mathbf{x},\mathbf{R}_{J'})\right) + \frac{\partial V_c(\mathbf{x},\mathbf{R})}{\partial \mathbf{R}_{J'}}\left(\tilde{b}(\mathbf{x},\mathbf{R}) + b(\mathbf{x},\mathbf{R})\right) \\
&\quad \left. + b_{J'}(\mathbf{x},\mathbf{R}'_J)\frac{\partial V_{J'}(\mathbf{x},\mathbf{R}_{J'})}{\partial \mathbf{R}_{J'}} - \tilde{b}_{J'}(\mathbf{x},\mathbf{R}_{J'})\frac{\partial \tilde{V}_{J'}(\mathbf{x},\mathbf{R}_{J'})}{\partial \mathbf{R}_{J'}}\right] \mathrm{d}\mathbf{x} \\
&= \frac{1}{2}\sum_{J'}\int_\Omega \left[\nabla\tilde{b}_{J'}(\mathbf{x},\mathbf{R}_{J'})\left(V_c(\mathbf{x},\mathbf{R}) - \tilde{V}_{J'}(\mathbf{x},\mathbf{R}_{J'})\right)\right. \\
&\quad + \nabla b_{J'}(\mathbf{x},\mathbf{R}_{J'})\left(V_c(\mathbf{x},\mathbf{R}) + V_{J'}(\mathbf{x},\mathbf{R}_{J'})\right) + \nabla V_{c,J'}(\mathbf{x},\mathbf{R}_{J'})\left(\tilde{b}(\mathbf{x},\mathbf{R}) + b(\mathbf{x},\mathbf{R})\right) \\
&\quad \left. + b_{J'}(\mathbf{x},\mathbf{R}_{J'})\nabla V_{J'}(\mathbf{x},\mathbf{R}_{J'}) - \tilde{b}_{J'}(\mathbf{x},\mathbf{R}_{J'})\nabla\tilde{V}_{J'}(\mathbf{x},\mathbf{R}_{J'})\right] \mathrm{d}\mathbf{x}\,,
\end{aligned}$$

where the summation J' is over J^{th} atom and its periodic images. Additionally,

$$\nabla V_{c,J'}(\mathbf{x},\mathbf{R}_{J'}) = \nabla\tilde{V}_{J'}(\mathbf{x},\mathbf{R}_{J'}) - \nabla V_{J'}(\mathbf{x},\mathbf{R}_{J'}). \tag{68}$$

It is important to note that even with these corrections to the energy and forces, the overall OF-DFT formulation maintains its linear-scaling with respect to the number of atoms.

APPENDIX C

CONJUGATE GRADIENT METHOD FOR OF-DFT

In Algorithm 1, we present the implemented conjugate gradient method to solve the variational problem in Eqn. 43. This differs from the standard non-linear conjugate gradient method [52] in that it is able to handle the constraints $\mathcal{C}(u) = 0$ and $u \geq 0$.

Algorithm 1: Non-linear conjugate gradient method for OF-DFT

Input: u_0, $\mathbf{R}$, V_{LR} and $N_{restart}$

$q = 0$

repeat

  $\eta_q = \frac{1}{N_e}\langle u_q, \mathcal{H}u_q \rangle$, where $\langle ., . \rangle$ denotes the inner product

  $r_q = -2(\mathcal{H}u_q - \eta_q u_q)$

  $\xi = \frac{\langle r_q - r_{q-1}, r_q \rangle}{\langle r_{q-1}, r_{q-1} \rangle}$

  if $q = mN_{restart}$ $(m \in \mathbb{N})$ *or* $\xi \leq 0$ **then**

    $d_q = r_q$

  else

    $d_q = r_q + \xi d_{q-1}$

  $s = \arg\inf_{s \in \mathbb{R}} \hat{\mathcal{E}}\left(\sqrt{N_e}\frac{u_q - s r_q}{\|u_q - s r_q\|}, \mathbf{R}, V_{LR}\right)$

  $u_{q+1} = \sqrt{N_e}\frac{u_q - s r_q}{\|u_q - s r_q\|}$

  $q = q + 1$

until $\|r\|^2 < tol$;

Output: $u = u_q$

APPENDIX D

ANDERSON MIXING

The fixed-point problem in Eqn. 42 can be rewritten as

$$f(V_{LR}) = 0\,, \quad f(V_{LR}) = \mathcal{V}\big[\mathcal{U}(V_{LR})\big] - V_{LR}\,. \tag{69}$$

This equation can be solved using an iteration of the form [15, 41]

$$V_{LR,k+1} = V_{LR,k} - C_k f(V_{LR,k})\,, \tag{70}$$

where C_k is chosen to approximate the inverse Jacobian. In multi-secant type methods, it is common to set C_k to the solution of the constrained minimization problem [15, 41]

$$\min_C \frac{1}{2}\|C - C_{k-1}\|_2^2 \quad \text{s.t.} \quad S_k = CY_k\,, \tag{71}$$

where

$$\begin{aligned} S_k &= [V_{LR,k-m+1} - V_{LR,k-m}, \ldots, V_{LR,k} - V_{LR,k-1}]\,, \\ Y_k &= [f(V_{LR,k-m+1}) - f(V_{LR,k-m}), \ldots, f(V_{LR,k}) - f(V_{LR,k-1})]\,. \end{aligned}$$

In the above equations, m represents the mixing history. The solution of this variational problem is

$$C_k = C_{k-1} + (S_k - C_{k-1}Y_k)(Y_k^T Y_k)^{-1} Y_k^T\,. \tag{72}$$

In the specific case of Anderson mixing [1], C_{k-1} is set to $-\zeta I$, where I is a $m \times m$ identity matrix. This leads to the following update formula within the fixed-point iteration

$$V_{LR,k+1} = V_{LR,k} + \zeta f(V_{LR,k}) - (S_k + \zeta Y_k)(Y_k^T Y_k)^{-1} Y_k^T f(V_{LR,k})\,. \tag{73}$$

REFERENCES

[1] Anderson, D. G., "Iterative procedures for nonlinear integral equations," *Journal of the ACM (JACM)*, vol. 12, no. 4, pp. 547–560, 1965.

[2] Balay, S., Brown, J., , Buschelman, K., Eijkhout, V., Gropp, W. D., Kaushik, D., Knepley, M. G., McInnes, L. C., Smith, B. F., and Zhang, H., "PETSc users manual," Tech. Rep. ANL-95/11 - Revision 3.4, Argonne National Laboratory, 2013.

[3] Balay, S., Gropp, W. D., McInnes, L. C., and Smith, B. F., "Efficient management of parallelism in object oriented numerical software libraries," in *Modern Software Tools in Scientific Computing* (Arge, E., Bruaset, A. M., and Langtangen, H. P., eds.), pp. 163–202, Birkhäuser Press, 1997.

[4] Benguria, R., Brezis, H., and Lieb, E., "The thomas-fermi-von weizscker theory of atoms and molecules," *Communications in Mathematical Physics*, vol. 79, no. 2, pp. 167–180, 1981.

[5] Benzi, M., Boito, P., and Razouk, N., "Decay properties of spectral projectors with applications to electronic structure," *SIAM Review*, vol. 55, no. 1, pp. 3–64, 2013.

[6] Blanc, X. and Cances, E., "Nonlinear instability of density-independent orbital-free kinetic-energy functionals," *The Journal of Chemical Physics*, vol. 122, no. 21, p. 214106, 2005.

[7] Bowler, D. R. and Miyazaki, T., "$\mathcal{O}(N)$ methods in electronic structure calculations," *Reports on Progress in Physics*, vol. 75, no. 3, p. 036503, 2012.

[8] Cances, E., Chakir, R., and Maday, Y., "Numerical analysis of the planewave discretization of some orbital-free and kohn-sham models.," *ESAIM-Mathematical Modelling and Numerical Analysis-Modelisation Mathematique et Analyse Numerique*, vol. 46, no. 2, pp. 341 – 388, 2012.

[9] Cances, E., Bris, C. L., and Lions, P.-L., "Molecular simulation and related topics: some open mathematical problems," *Nonlinearity*, vol. 21, no. 9, p. T165, 2008.

[10] Carling, K. M. and Carter, E. A., "Orbital-free density functional theory calculations of the properties of al, mg and al–mg crystalline phases," *Modelling and Simulation in Materials Science and Engineering*, vol. 11, no. 3, p. 339, 2003.

[11] Ceperley, D. M. and Alder, B. J., "Ground state of the electron gas by a stochastic method," *Phys. Rev. Lett.*, vol. 45, pp. 566–569, Aug 1980.

[12] Choly, N. and Kaxiras, E., "Kinetic energy density functionals for non-periodic systems," *Solid State Communications*, vol. 121, no. 5, pp. 281 – 286, 2002.

[13] Ciarlet, P., Lions, J., and Le Bris, C., *Handbook of Numerical Analysis : Special Volume: Computational Chemistry (Vol X)*. North-Holland, 2003.

[14] Cooley, J. and Tukey, J., "An algorithm for the machine calculation of complex fourier series.," *Mathematics of Computation*, vol. 19, no. 90, p. 297, 1965.

[15] Fang, H.-r. and Saad, Y., "Two classes of multisecant methods for nonlinear acceleration," *Numerical Linear Algebra with Applications*, vol. 16, no. 3, pp. 197–221, 2009.

[16] Fermi, E., "Un metodo statistice per la determinazione di alcune propieta dellatomo," *Rend. Accad. Nazl. Lincei*, vol. 6, pp. 602–607, 1927.

[17] Finnis, M., *Interatomic forces in condensed matter*. Oxford University Press, 2003.

[18] Garcia-Cervera, C. J., "An efficient real space method for Orbital-Free Density-Functional Theory," *Communications in Computational Physics*, vol. 2, pp. 334–357, APR 2007.

[19] Gavini, V. The authors were exploring similar ideas when the approach was suggested in private communication., 2014.

[20] Gavini, V., Bhattacharya, K., and Ortiz, M., "Quasi-continuum orbital-free density-functional theory: A route to multi-million atom non-periodic DFT calculation," *Journal of the Mechanics and Physics of Solids*, vol. 55, no. 4, pp. 697 – 718, 2007.

[21] Gavini, V., Knap, J., Bhattacharya, K., and Ortiz, M., "Non-periodic finite-element formulation of Orbital-free density functional theory," *Journal of the Mechanics and Physics of Solids*, vol. 55, no. 4, pp. 669 – 696, 2007.

[22] Ghosh, S. and Suryanarayana, P., "Higher-order finite-difference formulation of periodic orbital-free density functional theory," *arXiv preprint arXiv:1412.8250*, 2014.

[23] Gillan, M., "Calculation of the vacancy formation energy in aluminium," *Journal of Physics: Condensed Matter*, vol. 1, no. 4, p. 689, 1989.

[24] Goedecker, S., "Linear scaling electronic structure methods," *Rev. Mod. Phys.*, vol. 71, pp. 1085–1123, Jul 1999.

[25] Golub, G. H. and Van Loan, C. F., *Matrix computations*, vol. 3. JHU Press, 2012.

[26] Goodwin, L., Needs, R. J., and Heine, V., "A pseudopotential total energy study of impurity-promoted intergranular embrittlement," *Journal of Physics: Condensed Matter*, vol. 2, no. 2, p. 351, 1990.

[27] Gropp, W., Lusk, E., and Skjellum, A., *Using MPI: portable parallel programming with the message-passing interface*, vol. 1. MIT press, 1999.

[28] Ho, G., Ong, M. T., Caspersen, K. J., and Carter, E. A., "Energetics and kinetics of vacancy diffusion and aggregation in shocked aluminium via orbital-free density functional theory," *Physical Chemistry Chemical Physics*, vol. 9, no. 36, pp. 4951–4966, 2007.

[29] Ho, G. S., Ligneres, V. L., and Carter, E. A., "Introducing PROFESS: A new program for orbital-free density functional theory calculations," *Computer Physics Communications*, vol. 179, no. 11, pp. 839 – 854, 2008.

[30] Hohenberg, P. and Kohn, W., "Inhomogeneous electron gas," *Physical Review*, vol. 136, no. 3B, pp. B864–B871, 1964.

[31] Huang, C. and Carter, E. A., "Transferable local pseudopotentials for magnesium, aluminum and silicon," *Physical Chemistry Chemical Physics*, vol. 10, no. 47, pp. 7109–7120, 2008.

[32] Hung, L. and Carter, E. A., "Accurate simulations of metals at the mesoscale: Explicit treatment of 1 million atoms with quantum mechanics," *Chemical Physics Letters*, vol. 475, no. 4, pp. 163–170, 2009.

[33] Hung, L., Huang, C., and Carter, E. A., "Preconditioners and electron density optimization in orbital-free density functional theory," *Communications in Computational Physics*, vol. 12, no. 1, p. 135, 2012.

[34] Hung, L., Huang, C., Shin, I., Ho, G. S., Ligneres, V. L., and Carter, E. A., "Introducing PROFESS 2.0: A parallelized, fully linear scaling program for orbital-free density functional theory calculations," *Computer Physics Communications*, vol. 181, no. 12, pp. 2208 – 2209, 2010.

[35] Jiang, H. and Yang, W., "Conjugate-gradient optimization method for orbital-free density functional calculations," *The Journal of Chemical Physics*, vol. 121, no. 5, pp. 2030–2036, 2004.

[36] Jordan, D. and Mazziotti, D., "Spectral differences in real-space electronic structure calculations," *The Journal of Chemical Physics*, vol. 120, no. 2, pp. 574–578, 2003.

[37] Karasiev, V. V., Sjostrom, T., and Trickey, S., "Finite-temperature orbital-free dft molecular dynamics: coupling profess and quantum espresso," *arXiv preprint arXiv:1406.0835*, 2014.

[38] Kohn, W., "Nobel lecture: Electronic structure of matter¯wave functions and density functionals," *Rev. Mod. Phys.*, vol. 71, pp. 1253–1266, Oct 1999.

[39] Kohn, W. and Sham, L. J., "Self-consistent equations including exchange and correlation effects," *Physical Review*, vol. 140, no. 4A, pp. A1133–A1138, 1965.

[40] LeVeque, R., *Finite Difference Methods for Ordinary and Partial Differential Equations: Steady-state and Time-Dependent Problems*. SIAM, 2007.

[41] Lin, L. and Yang, C., "Elliptic preconditioner for accelerating the self-consistent field iteration in kohn–sham density functional theory," *SIAM Journal on Scientific Computing*, vol. 35, no. 5, pp. S277–S298, 2013.

[42] Martin, R., *Electronic Structure: Basic theory and practical methods*. Cambridge University Press, 2004.

[43] Mazziotti, D. A., "Spectral difference methods for solving differential equations," *Chemical physics letters*, vol. 299, no. 5, pp. 473–480, 1999.

[44] Motamarri, P., Iyer, M., Knap, J., and Gavini, V., "Higher-order adaptive finite-element methods for orbital-free density functional theory," *Journal of Computational Physics*, vol. 231, no. 20, pp. 6596 – 6621, 2012.

[45] Parr, R. and Yang, W., *Density-functional theory of atoms and molecules*. Oxford University Press, 1989.

[46] Pask, J. E. and Sterne, P. A., "Real-space formulation of the electrostatic potential and total energy of solids," *Phys. Rev. B*, vol. 71, p. 113101, Mar 2005.

[47] Payne, M. C., Teter, M. P., Allan, D. C., Arias, T., and Joannopoulos, J., "Iterative minimization techniques for ab initio total-energy calculations: molecular dynamics and conjugate gradients," *Reviews of Modern Physics*, vol. 64, no. 4, pp. 1045–1097, 1992.

[48] Perdew, J. P. and Zunger, A., "Self-interaction correction to density-functional approximations for many-electron systems," *Phys. Rev. B*, vol. 23, pp. 5048–5079, May 1981.

[49] Pickett, W. E., "Pseudopotential methods in condensed matter applications," *Computer Physics Reports*, vol. 9, no. 3, pp. 115–197, 1989.

[50] Press, W. H., Teukolsky, S. A., Vetterling, W. T., and Flannery, B. P., *Numerical recipes 3rd edition: The art of scientific computing*. Cambridge University press, 2007.

[51] Saad, Y. and Schultz, M. H., "Gmres: A generalized minimal residual algorithm for solving nonsymmetric linear systems," *SIAM Journal on scientific and statistical computing*, vol. 7, no. 3, pp. 856–869, 1986.

[52] Shewchuk, J. R., "An introduction to the conjugate gradient method without the agonizing pain," 1994.

[53] Sjostrom, T. and Daligault, J., "Fast and accurate quantum molecular dynamics of dense plasmas across temperature regimes," *Physical Review Letters*, vol. 113, no. 15, p. 155006, 2014.

[54] Suryanarayana, P., Bhattacharya, K., and Ortiz, M., "A mesh-free convex approximation scheme for kohn-sham density functional theory," *Journal of Computational Physics*, vol. 230, no. 13, pp. 5226 – 5238, 2011.

[55] Suryanarayana, P., Bhattacharya, K., and Ortiz, M., "Coarse-graining kohn-sham density functional theory," *Journal of the Mechanics and Physics of Solids*, vol. 61, no. 1, pp. 38 – 60, 2013.

[56] Suryanarayana, P., Gavini, V., Blesgen, T., Bhattacharya, K., and Ortiz, M., "Non-periodic finite-element formulation of Kohn-Sham density functional theory," *Journal of the Mechanics and Physics of Solids*, vol. 58, no. 2, pp. 256 – 280, 2010.

[57] Suryanarayana, P. and Phanish, D., "Augmented Lagrangian formulation of Orbital-free density functional theory," *Journal of Computational Physics*, vol. 275, pp. 524–538, 2014.

[58] Teter, M. P., Payne, M. C., and Allan, D. C., "Solution of Schrödinger's equation for large systems," *Physical Review B*, vol. 40, no. 18, p. 12255, 1989.

[59] Thomas, L. H., "The calculation of atomic fields," *Mathematical Proceedings of the Cambridge Philosophical Society*, vol. 23, pp. 542–548, 1 1927.

[60] Wang, L.-W. and Teter, M. P., "Kinetic-energy functional of the electron density," *Phys. Rev. B*, vol. 45, pp. 13196–13220, Jun 1992.

[61] Wang, Y. A. and Carter, E. A., "Orbital-free kinetic-energy density functional theory," in *Theoretical Methods in Condensed Phase Chemistry* (Schwartz, S. D., ed.), vol. 5 of *Progress in Theoretical Chemistry and Physics*, pp. 117–184, Springer Netherlands, 2002.

[62] Wang, Y. A., Govind, N., and Carter, E. A., "Orbital-free kinetic-energy functionals for the nearly free electron gas," *Phys. Rev. B*, vol. 58, pp. 13465–13471, Nov 1998.

[63] Wang, Y. A., Govind, N., and Carter, E. A., "Orbital-free kinetic-energy density functionals with a density-dependent kernel," *Phys. Rev. B*, vol. 60, pp. 16350–16358, Dec 1999.

[64] Weizsacker, C., "Zur theorie der kernmassen," *Zeitschrift fur Physik*, vol. 96, no. 7-8, pp. 431–458, 1935.

[65] Xia, J., Huang, C., Shin, I., and Carter, E. A., "Can orbital-free density functional theory simulate molecules?," *The Journal of Chemical Physics*, vol. 136, no. 8, p. 084102, 2012.

[66] Zhou, B., Ligneres, V. L., and Carter, E. A., "Improving the orbital-free density functional theory description of covalent materials," *The Journal of Chemical Physics*, vol. 122, no. 4, p. 044103, 2005.